COUPLING OF ISOTHERMAL MODELS IN GAS NETWORKS

by

Jose Eduardo CEJUDO GRANO DE ORO

In partial fulfillment of the requirements for the degree of

Master of Science in Applied Mathematics

at the Delft University of Technology, to be defended publicly on Friday July 19, 2019 at 11:00 AM.

Student number: 4958381

Thesis commitee:

Dr. ir. J.E. Romate,	TU Delft & Shell Global Solutions International (supervisor)
Prof dr. ir. C. Vuik,	TU Delft
Dr. ir. H.M. Schuttelaars,	TU Delft

An electronic version of this dissertation is available at
http://repository.tudelft.nl/.

CONTENTS

SUMMARY

This work is concerned with the simulation of gas networks using a hybrid modeling approach where different pipes are described with models belonging to the isothermal model hierarchy. It makes special emphasis in the coupling of algebraic and transient models and their effects in both steady-state and transient regime.
The transient behavior of simple networks is studied in both non-dissipative and dissipative regime with a perturbation analysis. Physical effects concerning transmission and reflection of perturbations are studied both numerical and analytically. The transient response of the algebraic model is studied and compared with the results of numerical experiments. Finally a perturbative approach for computing the attenuation coefficient for dissipative transport is proposed and the analytical results are compared with the numerical experiments.

ACKNOWLEDGEMENTS

This thesis has been written as the graduation project for the Computer Simulations for Science and Engineering (COSSE) master's program. For the past two years I had the chance to study at TU Berlin and TU Delft, being an exciting period of learning and growth both professional and personally. I would like to thank the coordinators of the program, in particular Reinhard Nabben (TU Berlin), Kees Vuik (TU Delft) and Michael Hanke (KTH) for orientation and guidance throughout the program.
A special mention goes to my thesis supervisor Johan Romate for fruitful conversations, dedication and advice during my master's thesis.
None of this would have been possible without the support and love of my family, to whom I owe my past, present and future accomplishments.

Jose Eduardo Cejudo, Delft, July 2019

1

INTRODUCTION

Natural gas is a fossil fuel created by the storage and anaerobic decomposition of organic material in the upper crust of the Earth during millions of year under high pressure and temperature conditions. It is mainly composed of alkanes, in particular hydrocarbons. Methane is the dominant component, and its relatively high concentration is due to the past life on Earth. Other gases are also present in smaller concentrations such as Helium, Nitrogen and Carbon dioxide. Natural gas is currently one of the main natural resources being its main usage for energy generation. Its energy density is significantly smaller than other fossil fuels, although its ease of storage and transport has made it one of the main energy sources. Its consumption is wide accross industries and private households, making the demand for natural gas global. Since the main sources are localized in a few areas around the world, the transport of gas has become an important issue for the global economy [1].

Transport of natural gas is traditionally done by systems of pipeline networks, also known as transmission lines. These are network structures composed by pipes, achieving transport by pressure differences. The size of the networks ranges from tens to hundreds of pipes and elements, making the study of these systems a complex task. Although the mathematical models for describing transport of gas in a single pipe are well understood, the problem rapidly becomes analytically intractable when more elements are added. Therefore, numerical simulation has become a relevant tool for the study of gas pipeline networks, allowing to understand the detailed behavior of the system and to optimize the transport according to environmental, economical and energetic constraints.

The mathematical models used for the simulation of gas transport stem from the more general framework of fluid dynamics. These constitute a system of partial differential equations (PDEs) in space and time, to which standard discretization methods based on finite differences, elements and volumes can be applied. The time dependence of the model allows for the transient simulation of the system, i.e., it allows to study its dynamical behavior. Although this approach leads to highly accurate results, its computational cost is usually high, making simulations very demanding of computational

resources for large networks. An alternative approach is to use algebraic equations for describing the transport. The advantage of this is that no discretization is required and it is significantly easier to obtain a solution to the transport problem. However, the accuracy of the solution might be compromised by the simplicity of the model.
The goal of this thesis is to study the hybrid modeling of gas networks using both transient and algebraic models. This is equivalent to having a high resolution description in the pipes described by the transient model and a low resolution for the pipes described by the algebraic model. It becomes interesting to study the approximation errors induced by the simplicity of the algebraic model, as well as the differences in dynamical behavior when coupling a transient and algebraic model.
This project aims to answer the following research questions:

- What is the effect of using the algebraic model for the hybrid modeling of gas networks?
- How does the algebraic model affect the transient behavior of the network when coupled with transient models?
- Is it possible to derive an analytical model for describing the transient behavior of hybrid networks in both non dissipative and dissipative transport?

The organization of the document is as follows: Chapter 2 serves as an introduction to the fundamentals of gas transport. The physical characterization of the gas will be presented, an analysis and comparison of several friction factors will be introduced, and the transport equations will be derived. Chapter 3 will focus on the isothermal models considered in this study, presenting the model hierarchy and comparing the different models for a single pipe. Chapter 4 contains a review of numerical methods for solving hyperbolic problems, and discusses an implicit box scheme suitable for subsonic flow which will be the method used for the numerical simulations. Chapter 5 introduces the coupling conditions for isothermal models, as well as the discretized transport equations and model coupling for benchmark networks. A comparison of hybrid models in simple networks for steady-state regime will be discussed. Chapter 6 focuses on transient phenomenology in networks using a perturbative approach. A special emphasis in analytical results is made, by discussing the calculation of transmission and reflection coefficients and the response of the algebraic model to perturbations. In the case of non dissipative transport a comparison of analytical and numerical solutions focusing on the effects of using the algebraic model coupled with transient models is carried out. Finally the transport including friction will be studied by a perturbation analysis for computing analytically the decay coefficient due to friction and comparing with the results of the numerical experiments.

2

FUNDAMENTALS OF GAS TRANSPORT

For studying the transport of gas in pipeline networks it becomes necessary to understand the physical characterization of the gas as well as the transport model governing the static and dynamical behavior of gas in pipes. The theoretical framework adopted for this study is fluid dynamics. Fluids can be either gas or liquids, being distinguishable through their thermodynamical properties. In particular, gas usually has low density and viscosity compared to liquids, and it is considered as a compressible fluid. This chapter covers the mathematical modeling of gas with special emphasis on the equation of state, compressibility factor and the friction coefficient between the gas and the pipes. A brief introduction to the Navier-Stokes equations is presented, being a general framework for the description of fluid dynamics. This will facilitate the understanding of the transport models relevant for this study which are discussed in subsequent chapters.

2.1. GAS PROPERTIES AND EQUATION OF STATE

Gas is defined as one of the fundamental states of matter. Its building blocks can be either individual atoms or molecules of the same or different elements, with the intermolecular bonds usually weak compared to liquids and solids. Gases don't have any specific shape, and they expand until occupying the entire volume of the container. Due to the extremely large number of particles, an exact microscopic study of gases is unfeasible, even though the laws governing the microscopic behavior are well understood. However, it is possible to start from the fundamental microscopic system and apply techniques from statistical mechanics to obtain macroscopic laws. Historically these macroscopic laws were empirically discovered first, forming part of classical thermodynamics. Later these laws were theoretically justified thanks to advances in statistical physics.
The macroscopic model of gases establishes relations between the variables associ-

ated to the system, being these the pressure p, density ρ and temperature T. Classically there has been a clear distinction between the so called ideal and real gas models. The ideal gas models are simplified models in which the following two assumptions are made:

- The volume of the molecules is negligible compared to the gas volume, being the molecules treated as zero-dimensional entities (points in the mathematical sense).
- The attractive and repulsive interactions between the molecules is not considered, and the collisions between them are assumed elastic, i.e., without loss of energy.

Although these assumptions might work in certain situations, it is clear that they limit significantly the applicability of the model. If the assumptions for ideal gases are dropped, then the problem becomes to model a real gas.
Both ideal and real gas models share the so called equation of state, being an algebraic relation between the thermodynamic variables of the system and given by:

$$p = R\rho T z\left(p, T\right) \tag{2.1}$$

where $R = 8.314\,\mathrm{J\,mol^{-1}\,K^{-1}}$ is the gas constant and z is the so called compressibility factor. More details will be provided in the next subsection.

2.2. COMPRESSIBILITY FACTOR

The compressibility factor is formally defined as the ratio of the gas volume at a given pressure and temperature to the volume of the gas if it were an ideal gas at the same pressure and temperature. From the definition it is clear that z is equal to 1 for ideal gases, whereas it is a function of the pressure and temperature for real gases.
The ideal gas approximation has been demonstrated to be suitable for gases in low density conditions, given by low pressure and high temperature [2]. The error made by using the aforementioned approximations is negligible for a wide variety of gases and the ideal gas approximation is a widely adopted model. However, the values of pressure in typical gas networks is relatively high and therefore compressibility effects need to be taken into account. In the remaining of this study the gas will be modeled as a real gas unless stated otherwise.
For a real gas the derivation of the expression for the compressibility factor can be approximated by the virial theorem, which expresses z as a power series in p and T [3]:

$$z = 1 + \sum_{i=1}^{\infty} B_{i+1}\left(T\right)\left(\frac{N}{V}\right)^{i} = 1 + \sum_{i=1}^{\infty} \tilde{B}_{i+1}\left(T\right) p^{i} \tag{2.2}$$

where B_i are the so called virial coefficients. The dependence of $\frac{N}{V}$ with p given by the equation of state has been used for expressing the series as powers of the pressure. Using this approach several equations of state can be derived.
The choice regarding the equation of state is expected to affect the modeling of the gas and therefore the overall behavior of the system. However, after a comparison between

several equations of state for non-isothermal flow in a single pipeline carried out in [4], it was concluded that both steady state and transient behavior don't depend strongly on the particular choice for the equations of state considered.
One of the most widely employed expressions for the compressibility factor was proposed by the American Gas Associacion, and it is known as the AGA compressibility factor:

$$z(p,T) = 1 + 0.257\frac{p}{p_c} - 0.533\frac{pT}{p_c T_c}. \tag{2.3}$$

where p_c and T_c are the critical pressure and temperature of the gas considered. This will be the expression used in this study.

2.3. FRICTION FACTOR

When the gas is transported through a pipe the input pressure does not remain constant along the pipe, but there exists a pressure drop. This pressure drop is mainly due to two reasons: gravity effects and friction. Gravity effects can affect the pressure of fluids in pipes with non-zero slope. The inclination of the pipe produces an increase of pressure in those parts of the pipe with small elevation, and a decrease in the regions with higher elevation. In this subsection we are focused on the pressure drop due to friction between the pipes and the fluid, and this will be formally described by means of the Darcy friction coefficient λ.
Viscosity is a property of fluids that quantifies the resistance to flow due to frictional forces. For the purpose of this thesis only the friction between the fluid and the inner surface of the pipe is considered. The effects of the viscosity yield two flow regimes, namely laminar and turbulent. Laminar flow consists of the fluid traveling in layers, whereas in the case of turbulent flow instabilities arise.
A common metric to assess the turbulence regime of fluids is the Reynolds number. In the case of gas flow in cylindrical pipes, the Reynolds number will depend on the viscosity coefficient of the fluid as well as on geometrical parameters of the pipe as:

$$\mathrm{Re}(q) = \frac{D}{A\eta}|q| \tag{2.4}$$

where D is the diameter of the pipe, $A = \pi\left(\frac{D}{2}\right)^2$ the cross-sectional area, η is the viscosity coefficient and $q = A\rho v$ is the mass flow. The convention is that the flow will be considered laminar if $\mathrm{Re} < 2000$, partially turbulent if $2000 < \mathrm{Re} < 4000$, and fully turbulent if $4000 < \mathrm{Re}$.
Apart from the viscosity coefficient present in the Reynolds number, the roughness of the inner surface of the pipes is also expected to contribute to the pressure loss due to friction. In order to account for frictional effects between the fluid and the inner pipe an additional roughness coefficient k is introduced.
This section introduces several friction factors widely used in modeling the friction between the gas and pipes. An analysis and comparison for different turbulence regimes and pipe parameters will be performed. For a thorough review of the existing frictions factors the reader is referred to [5].

The complexity of laminar flow is significantly smaller than for turbulent flow, and therefore some simple expressions for the friction factor have been proposed for this regime. The first one only depends on the Reynolds number, being inversely proportional to it:

$$\lambda = \frac{64}{\mathrm{Re}} \tag{2.5}$$

For small values of the Reynolds number the friction factor is maximal, decreasing for large Reynolds numbers. This is analogous to the static friction coefficient being higher than the dynamical friction coefficient in classical mechanics.
Another friction factor is due to Weymouth. It has no dependency on the Reynolds number, only on the diameter of the pipe:

$$\frac{1}{\sqrt{\lambda}} = 3.2605 D^{\frac{1}{6}} \tag{2.6}$$

The Weymouth friction factor is often larger than the friction factors from the other laws presented, and particularly when the flow is turbulent as it will be seen later in the forthcoming analysis.
In general the friction factor will have complicated dependencies with the Reynolds number, the diameter of the pipe and the roughness coefficient. The friction factors presented next aim to capture these complicated dependencies and are valid for both laminar and turbulent regime. The Colebrook-White friction factor depends on k, Re and D as follows:

$$\frac{1}{\sqrt{\lambda}} = -2\log_{10}\left(\frac{k}{3.7D} + \frac{2.51}{\mathrm{Re}\sqrt{\lambda}}\right) \tag{2.7}$$

Notice that the friction factor is given implicitly by the previous relation since it is necessary to solve a non linear equation to obtain λ. The usual approach is to assume an initial friction factor and iterate the previous equation with the updated friction factor until convergence. In the limit of $\mathrm{Re} \to \infty$, the Colebrook-White equation boils down to the friction factor proposed by the American Gas Association given by:

$$\frac{1}{\sqrt{\lambda}} = -2\log_{10}\left(\frac{k}{3.7D}\right) \tag{2.8}$$

In this case the friction factor can be evaluated directly. Another explicit expression is given by Chen's law [6], which has demonstrated being a quite accurate formula for the computation of the friction factor, and it is widely used for the simulation of gas transport in pipes [7]. It is given by:

$$\frac{1}{\sqrt{\lambda}} = -2\log_{10}\left(\frac{k}{3.7065D} - \frac{5.0425}{\mathrm{Re}}\log_{10}\left[\frac{(kD)^{1.1098}}{2.8257} + \frac{5.8506}{\mathrm{Re}^{0.8981}}\right]\right) \tag{2.9}$$

In Figure 2.1 a comparison of the friction factors presented in this section is included. Since they depend on the Reynolds number, friction coefficient and diameter of the pipes it is worth comparing the dependence of the friction factor with respect to these variables.

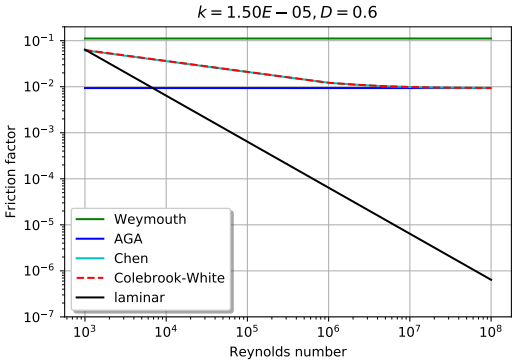

(a) Friction factor with respect the Reynolds number

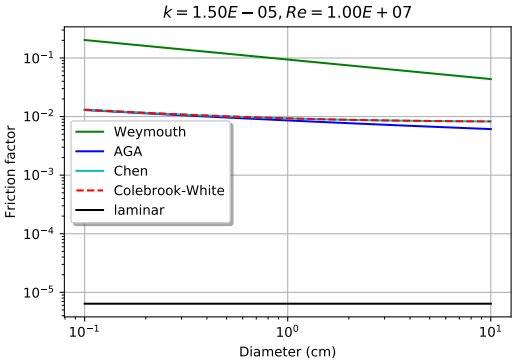

(b) Friction factor with respect to the pipe diameter

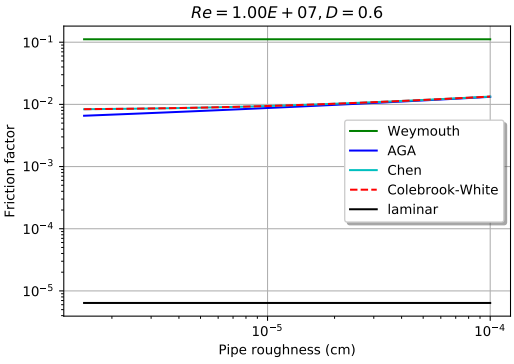

(c) Friction factor with respect to the pipe roughness

Figure 2.1: Dependency of the Darcy friction factors discussed in this chapter with respect to the Reynolds number, pipe diameter and roughness coefficient

In Figure 2.1a the pipe roughness k and the pipe diameter D are fixed, and the Reynolds number is varied from laminar to fully turbulent regime. The Weymouth and AGA friction factors remain constant since they only depend on D and k. On the other hand, Colebrook-White and Chen's law present a similar behavior ultimately converging to the same value for fully turbulent regime, together with the AGA equation. The resulting friction factor in the limit of fully turbulent regime is around one order of magnitude smaller than the Weymouth friction factor. It is also noticeable that the laminar friction factor reaches significantly lower values than the rest of the friction laws. However, since the validity regime of the laminar friction factor only holds for laminar flow ($Re < 2000$), the results for the laminar friction factor for fully turbulent regime are not realistic.
In Figure 2.1b the pipe roughness k and the Reynolds number Re are fixed. The chosen value for the Reynolds number corresponds to fully turbulent regime, being this a typical value in realistic applications. The pipe diameter D is varied in a range which scopes possible realistic values for the diameter of gas pipelines. Again Colebrook-White and Chen's law present a similar dependency, not showing an strong dependency on the diameter. On the other hand, the Weymouth friction factor decreases significantly with the diameter. Since the laminar friction factor only depends on the Reynolds number, its value remains constant and order of magnitude lower than the rest of friction models. This is due to the large value chosen for the Reynolds number.
Figure 2.1c contains a comparison of the friction factors presented when the pipe diameter D and Reynolds number Re are fixed to the previously mentioned values, and the pipe roughness coefficient k is varied. The Weymouth friction factor remains constant since it only depends on the diameter, and it is an order of magnitude larger than AGA, Chen and Colebrook-White models. These friction factors don't show a strong dependency on the roughness coefficient, remaining around the same order of magnitude for the values of k considered. As with varying diameter, the laminar friction factor remains constant in a value solely determined by the Reynolds number.
From the previous discussion we can conclude that both laminar and Weymouth friction factors don't provide with realistic models to account the friction between the gas and the pipes. They are rather simplistic models and their applicability is only suitable for very specific conditions which won't be meet in this study. It has also been observed that the rest of the models behave in a similar way and don't show strong dependencies with respect to their parameters. It is expected then that the friction factor when performing numerical simulations of pipes will be around 0.01. Due to the similarity of the AGA, Colebrook-White and Chen's models, it does not make a significant difference the model chosen. In the remainder of this thesis only Chen's friction factor will be considered.

2.4. TRANSPORT MODEL: NAVIER-STOKES EQUATIONS

Once the gas has been physically characterized by the equation of state and the friction between the gas and the pipes has been discussed, the next step is to find a model for the transport of gas. A general transport model for fluids is given by the Navier-Stokes equations, composed by a set of nonlinear system of partial differential equations (PDEs) which describe the macroscopic behavior of the fluid according with fun-

damental physical conservation laws, namely the conservation of the mass, momentum and energy.
Although a fully rigorous derivation of the Navier-Stokes equations is out of the scope of this study, it is convenient to briefly review the fundamental laws governing the transport. For a thorough study of the Navier-Stokes equations and related models see [8].

2.4.1. CONTINUITY EQUATION

For the derivation of the continuity equation it is useful to consider a finite control volume which is fixed in space, i.e., it doesn't move with the fluid. The continuity equation is based on a simple physical assumption: equality between the net mass flow out of the control volume through its surface and the time rate of decrease of mass inside the control volume. Denoting an infinitesimal unit of surface pointing outwards the volume element as $\vec{dS}$ and the velocity of the fluid pointing outwards the volume element as $\vec{V}$, an elemental mass flow going outwards of the control volume is given by $\rho\vec{V}\vec{dS}$. Therefore, the net mass flow going outwards from the control volume can be obtained by integrating over all the surface, obtaining $\int_S \rho\vec{V}\vec{dS}$. Since the total mass contained in the control volume is given by $\int_{\mathcal{V}} \rho d\mathcal{V}$, the time rate of decrease of flow can be written as $-\frac{\partial}{\partial t}\int_{\mathcal{V}} \rho d\mathcal{V}$. Thus, we can express the aforementioned conservation law as:

$$\frac{\partial}{\partial t}\int_{\mathcal{V}} \rho d\mathcal{V} + \int_S \rho\vec{V}\vec{dS} = 0 \tag{2.10}$$

The time derivative in the first term can be included inside the integral since the volume of the element is stationary. Moreover, Gauss's law can be applied in the second integral, expressing the integration over surface as an integration over volume. Particularizing the resulting expression to one dimension, the continuity equation in conservation form can be written as:

$$\frac{\partial \rho}{\partial t} + \frac{\partial(\rho V)}{\partial x} = 0 \tag{2.11}$$

2.4.2. MOMENTUM EQUATION

For the derivation of the momentum equation it is convenient to consider an infinitesimal element moving with the fluid, and it is assumed that this element satisfies the second Newton's law given by:

$$F_x = ma_x \tag{2.12}$$

This law simply states that the net force on the fluid element is equal to its mass times its acceleration. The forces on the element are of two types; body forces, which act directly on the volumetric mass of the element and can be written as $\rho f_x dxdydz$; and surface forces, which act on the surface of the element and are due to the pressure distribution around the fluid element. The total force on the fluid element can then be written as:

$$F_x = \left[-\frac{\partial p}{\partial x} + \rho f_x\right] dxdydz \tag{2.13}$$

Writing the differential of mass as $dm = \rho dxdydz$ and the acceleration as $a_x = \frac{Du}{Dt}$ where $\frac{D}{Dt}$ is the operator given by $\frac{D}{Dt} = \frac{\partial}{\partial t} + \vec{V}.\nabla$ and v is the velocity of the fluid, the momentum equation can be written in non conservative form:

$$\rho \frac{Dv}{Dt} = -\frac{\partial p}{\partial x} + \rho f_x \tag{2.14}$$

By rearranging some terms of the previous equation, using the vector identity $\rho\vec{V}.\nabla v = \nabla.\left(\rho v\vec{V}\right) - v\nabla.\left(\rho\vec{V}\right)$ and the continuity equation, the momentum equation for 1 dimensional flow is given by:

$$\frac{\partial(\rho v)}{\partial t} + \frac{\partial}{\partial x}\left(p + \rho v^2\right) = \rho f_x \tag{2.15}$$

2.4.3. ENERGY EQUATION

The moving fluid element will also be considered for the derivation of this expression. The physical assumption for the energy equation is of course the conservation of energy. Applied to the control volume, this conservation states that the rate of change of energy inside the element must be equal to the sum of the net flux of heat into the element and the rate of work done on the element due to body and surface forces.
We will start with the rate of work done. The physical definition of work is force times distance, and in the case of gases it can be expressed as pressure times the change in volume. The work done by the body forces is given by $\rho\vec{f}.\vec{V}dxdydz$, and the work done by surface forces will contain dependencies with respect to the pressure and velocity, being the net work done given by:

$$\left[-\frac{\partial(vp)}{\partial x} + \rho\vec{f}.\vec{V}\right]dxdydz \tag{2.16}$$

The net flux of heat will be due to the volumetric heating of the element plus the heating of the element due to thermal conduction. These two effects are gathered in the equation describing the net flux of heat:

$$\left[\rho\dot{q} - \left(\frac{\partial\dot{q}_x}{\partial x} + \frac{\partial\dot{q}_y}{\partial y} + \frac{\partial\dot{q}_z}{\partial z}\right)\right]dxdydz \tag{2.17}$$

where $\dot{q}$ is the rate of volumetric heat addition per unit mass and $\dot{q}_x = -k\frac{\partial T}{\partial x}$, leading to an expression for the next flux of heat:

$$\left[\rho\dot{q} + \frac{\partial}{\partial x}\left(k\frac{\partial T}{\partial x}\right) + \frac{\partial}{\partial y}\left(k\frac{\partial T}{\partial y}\right) + \frac{\partial}{\partial z}\left(k\frac{\partial T}{\partial z}\right)\right]dxdydz \tag{2.18}$$

Finally, the rate of energy change is due to the rate of change of internal plus kinetic energy, and it is given by: $\rho\frac{D}{Dt}\left(e + \frac{V^2}{2}\right)dxdydz$. Applying the conservation of energy, using the identity $\rho\vec{V}.\nabla e = \nabla.\left(\rho e\vec{V}\right) - e\nabla.\left(\rho\vec{V}\right)$, the one dimensional energy equation is given by:

$$\frac{\partial}{\partial t}\left[\rho\left(e + \frac{v^2}{2}\right)\right] + \frac{\partial}{\partial x}\left[\rho v\left(e + \frac{v^2}{2}\right)\right] = \rho\dot{q} + \frac{\partial}{\partial x}\left(k\frac{\partial T}{\partial x}\right) - \frac{\partial(vp)}{\partial x} + \rho\vec{f}.\vec{V} \tag{2.19}$$

2.4.4. NON ISOTHERMAL FLOW IN PIPES

The Navier Stokes equations discussed above comprise the continuity, momentum and energy equation for inviscid fluid. These are better known as the Euler equations. The external forces in the right hand side of the momentum and energy equation have been left unspecified. The friction between the fluid and the pipe wall can be included as an external force in the momentum equation, as well as the term responsible for gravity effects including the slope of the pipe. The Euler equations can be written as:

$$\frac{\partial \rho}{\partial t} + \frac{\partial}{\partial x}(\rho v) = 0, \tag{2.20a}$$

$$\frac{\partial}{\partial t}(\rho v) + \frac{\partial}{\partial x}(p + \rho v^2) = -\frac{\lambda}{2D}\rho v|v| - g\rho h', \tag{2.20b}$$

$$\frac{\partial}{\partial t}\Big(\rho(\frac{1}{2}v^2 + e)\Big) + \frac{\partial}{\partial x}\Big(\rho v(\frac{1}{2}v^2 + e) + pv\Big) = -\frac{k_w}{D}(T - T_w). \tag{2.20c}$$

where $e = c_v T + gh$ is the internal energy, which is a sum of thermal and potential energy. c_v is the heat capacity, k_w the heat conductivity coefficient, and T_w the wall temperature of the pipe. The right hand side of the energy equation represents the heat transfer between the gas and the internal wall of the pipe, and it is given by the heat transfer model [4, 9].

The unknowns for this system are the pressure, flow and temperature, and the complicated nonlinear relations between the variables makes this system of PDEs intractable by analytical methods, numerical methods being used instead. The computational complexity for solving this problem is high in general, so further simplifications can be made for making the problem more tractable numerically. This will be studied in the next chapter, where the assumption of constant temperature is made, giving rise to a family of isothermal models.

3

ISOTHERMAL MODELS

The transport model derived in the previous chapter depends on the pressure, flow and temperature of the gas. The dynamical behavior of the flow is described by a system of PDEs corresponding to the conservation of mass, momentum and energy. This model can be computationally expensive to solve due to the amount of variables, and therefore an important issue is the reduction of the complexity of the model. The most immediate question is the role played by the temperature in the transport. If the variation of temperature along the pipe doesn't have a relevant effect on the rest of variables it could be considered constant.
Reference [10] contains a comparison between non-isothermal and isothermal models for both steady state and transient regime of a benchmark network. The results of the study show that the assumption of constant temperature might compromise the accuracy of the description of the behavior for high values of the temperature, whereas for low values there is not a substantial difference between the isothermal and the non-isothermal models. The network considered is 122 km long and contains compressors for compensating the pressure losses due to friction.
The networks of interest in the current study will not contain compressors and will be significantly smaller, with a length of the order of a few kilometers. In order to compare the results for both non-isothermal and isothermal models the temperature, pressure

$L = 30$ km	$D = 0.6$ m	$p_{in} = 5 \times 10^6$ Pa
$q_{out} = 40$ kg/s	$T = 293$ K	$k =$ 1.5e-5
$\eta =$ 1e-5	$h' = 0$	$k_w = 0.0341$ W/(m K)
$c_v = 1850$ J/(kg K)	$\tau = 10$ s	$h = 50$ m
$p_c = 4.64 \times 10^6$ Pa	$T_c = 190.71K$	$c = 382.75$ m/s

Table 3.1: Parameters used for the comparison between non-isothermal and isothermal models

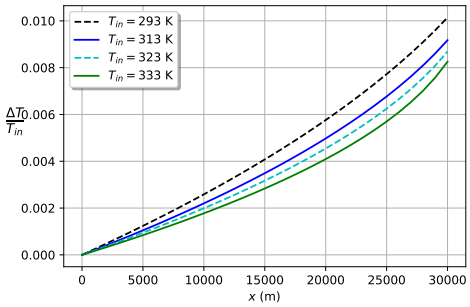

(a) Relative error for the temperature

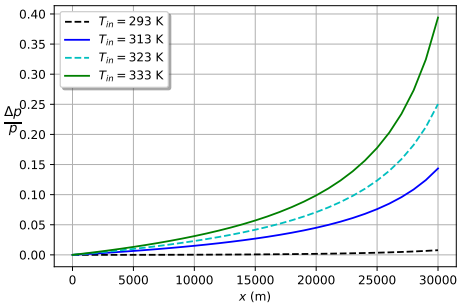

(b) Relative error for the pressure

Figure 3.1: Comparison of the temperature and pressure profile for the non-isothermal model and the isothermal Euler equations

and mass flow profiles for the two models will be compared for a single pipe. In particular, we are interested in the dependency on the temperature of the gas along the pipe, as well as the difference in the pressure and mass-flow rate profiles between the non-isothermal and isothermal case.

Apart from the transport model it is necessary to define boundary conditions. For a given network both input and output nodes can be defined, being the pressure specified at the input nodes and the mass-flow rate specified at the output nodes. In case of a single pipe the input node is at the beginning of the pipe, and the output node at the end. Therefore, the boundary conditions are the input pressure and the output flow. For the non-isothermal model, a boundary condition is also needed for the temperature. The temperature at the input nodes will therefore be a boundary condition as well.

The boundary and coupling conditions for gas networks will be discussed in detail in Chapter 5. The numerical simulations have been done using the methods described in Chapter 4 and the parameters used in the simulations are contained in Table 3.1, where τ and h are the time step and lattice spacing respectively. The results presented in this chapter correspond to the steady-state solution.

Figure 3.1a shows the relative error between the temperature profile along the pipe corresponding to the non-isothermal and isothermal model for four different input temperatures. It is observed that the maximum relative error is about 1% at the end of the pipe. It is also noted that this error is related to the minimum temperature considered. It can be concluded that the temperature profile remains almost constant along the pipe.

Since the variables of interest are the pressure and mass-flow rate, it becomes interesting to compare the spatial profiles of these variables for the non-isothermal and isothermal models. Figure 3.1b shows the relative error between the pressure profile of the non-isothermal and isothermal models. As expected the error grows towards the end of the pipe being zero at the entry node since the input pressure is fixed. It is observed that the higher the temperature, the higher the error. The maximum relative

error observed is around 40% for the highest temperature. Therefore, the assumption of constant temperature might compromise the accuracy of the model for high temperatures. However, in normal conditions the temperature of the gas rarely surpasses 300 K. It is clear from the graph that for temperatures below this value the relative error is smaller than 10%, and therefore the non-isothermal and isothermal models yield similar pressure profiles.
The relative error for the mass-flow rate profile is three orders of magnitude smaller than the relative error corresponding to the pressure profile. Since it provided little information it has been left out of this presentation. However, it is worth mentioning that for a given temperature the difference in mass-flow rate decreases towards the end of the pipe ultimately becoming zero since the flow rate at the end of the pipe is a boundary condition and therefore it is fixed. The numerical values of the relative error show that the difference between the mass-flow rate for the non-isothermal and isothermal case is negligible, the temperature not having a significant effect in the flow rate profile. Therefore, for the temperatures of interest it can be concluded that a variable temperature does not have significant effects in the pressure and mass-flow rate profiles. Moreover, the assumption of constant temperature makes the problem easier to solve computationally. The temperature can then be considered constant without a significant loss in accuracy and this will be the assumption in this study. This chapter introduces a family of isothermal models, namely the isothermal Euler equations, the semilinear and the algebraic model.

3.1. ISOTHERMAL EULER EQUATIONS

Under the assumption of isothermal regime thermal effects are neglected by considering the temperature as a constant. In this situation the energy equation becomes a trivial identity and it can be dropped, resulting in the system of equations:

$$\frac{\partial}{\partial t}\left(\frac{p}{RTz(p)}\right)+\frac{1}{A}\frac{\partial q}{\partial x}=0 \tag{3.1a}$$

$$\frac{1}{A}\frac{\partial q}{\partial t}+\frac{\partial p}{\partial x}+\frac{1}{A^2}\frac{\partial}{\partial x}\left(\frac{q^2RTz(p)}{p}\right)=-\frac{gh'}{RT}\frac{p}{z(p)}-\frac{RT}{2DA^2}\frac{z(p)\,q\,|q|\,\lambda(|q|)}{p} \tag{3.1b}$$

where the equation of state has been used as well as the definition of mass-flow rate. The variables in the isothermal case are the mass-flow rate q and pressure p. This is the model chosen for comparison with the non-isothermal model. One of the advantages of the isothermal Euler equations with respect to the non-isothermal model is that the isothermal approximation is significantly simpler than the temperature-dependent equations, leading to a lower computational complexity.
This fact together with the relatively weak dependence of the pressure and flow profiles on the temperature has made the isothermal Euler equations a well studied model for the transport of gas in pipelines, being the most common model for the study of gas networks. However, it can be difficult to study this model analytically.
This analytical intractability motivates the rest of this chapter in which approximations to the isothermal Euler equations are discussed, in particular the semilinear and alge-

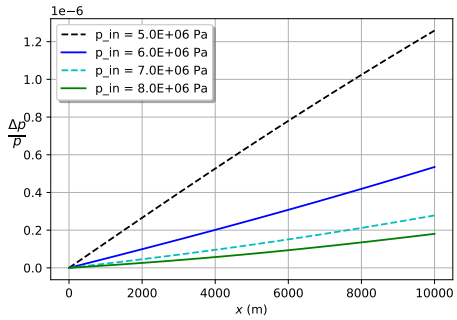

(a) Relative error for the pressure for several input pressures

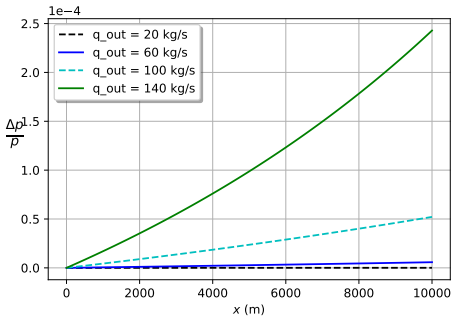

(b) Relative error for the pressure for several output flows

Figure 3.2: Comparison of the pressure profile for the isothermal Euler equations and semilinear model for several input pressures and output flows

braic model. The family of models derived from the Euler equations is also known as the model hierarchy [11], and the model adaptivity between models belonging to this hierarchy is a current research topic [12].

3.2. SEMILINEAR MODEL

The isothermal Euler equations provide with an accurate description of gas transport in pipelines and has been demonstrated to be equivalent to the temperature dependent model for the values of temperature, input pressure and output flow considered. However, it is complicated to treat analytically mainly due to the nonlinear term in the left hand side of the momentum equation.

The aforementioned nonlinear term is directly proportional to the mass-flow rate and inversely proportional to the pressure. Therefore, it is expected that for low values of flow rate and high values of pressure this term can be neglected. Assuming these conditions, the isothermal Euler equations can be approximated by:

$$\frac{\partial}{\partial t}\left(\frac{p}{RTz(p)}\right)+\frac{1}{A}\frac{\partial q}{\partial x}=0 \tag{3.2a}$$

$$\frac{1}{A}\frac{\partial q}{\partial t}+\frac{\partial p}{\partial x}=-\frac{gh'}{RT}\frac{p}{z(p)}-\frac{RT}{2DA^2}\frac{z(p)\,q|q|\lambda(|q|)}{p} \tag{3.2b}$$

This model is also called semilinear model [13] and, although the behavior of this model is expected to be similar to the isothermal Euler equations, it is significantly simpler and will allow to be treated analytically. In particular, a steady-state solution can be derived as seen in the next section. Moreover, it also allows analytical solutions for transient phenomena as will be demonstrated in Chapter 6.

Given the assumption of neglecting the aforementioned quadratic term, it is worth asking about the differences in behavior between the isothermal Euler equations and the

semilinear model. Figure (3.2) contains a comparison of the pressure profile for a single pipe using the isothermal Euler equations and the semilinear model in steady state for several input pressures and output flow rates.

For both variable input pressure and variable output flow rate it is observed that the relative error between the pressure profile corresponding to the isothermal Euler and semilinear model increases with the position of the pipe, being maximum at the rightmost end. As with the comparison between the temperature dependent model and the isothermal Euler equations this is due to the input pressure as a boundary condition.

It can be observed in Figure (3.2a) that in the case of variable input pressure the maximum relative error corresponds to the lowest input pressure considered. The error decreases with the input pressure, being minimum for the maximum value of the pressure considered. This is in agreement with the hypothesis of being the quadratic term in the isothermal Euler equations negligible for high values of pressure. Therefore, in this scenario the semilinear model becomes a good approximation to the isothermal Euler equations. The relative error corresponding to the flow rate profile does not show any particular dependence on the value of the input pressure and can be neglected due to its small order of magnitude.

In the case of variable output flow rate the opposite behavior is observed, the relative error for the pressure profile increasing with the output flow rate value. This can be justified by two reasons.

The most immediate one is the quadratic dependence of the nonlinear term with the mass-flow rate. If the pressure is kept constant and the mass-flow rate is increased, this term will increase as well, becoming more important and non negligible. On the other hand, for small values of flow it can be safely ignored. Therefore the error between the isothermal Euler equations and the semilinear model decreases with the value of the mass-flow rate.

The second reason has to do with the friction term at the right hand side of equation (5.9), which also depends quadratically on the mass-flow rate. For a single pipe the steady state mass-flow rate is constant and equal to the output flow rate, so increasing the flow rate at the end of the pipe also increases the flow profile and therefore the friction term. Higher friction causes a higher pressure loss, and therefore the pressure profile will have smaller values than in the case of non dissipative transport. Therefore, for high values of friction neglecting the quadratic term in the isothermal Euler equations is not such a suitable assumption, being this reflected in the increase in error between the isothermal and semilinear models. The error corresponding to the flow rate profile is maximum for the lowest value of output flow rate considered. It is observed, however, that it is three orders of magnitude smaller than the relative error corresponding to the pressure profile.

From the previous discussion it can be concluded that the pressure profile is relatively sensitive to values of the boundary conditions, being inversely proportional to the input pressure and directly proportional to the output flow rate. Given the order of magnitude of the resulting errors, it can be concluded that the semilinear model is a good approximation to the isothermal Euler equations for the input pressures, output flow rates and pipe parameters considered. Moreover, the semilinear model offers certain analytical advantages that will be considered in the rest of this study.

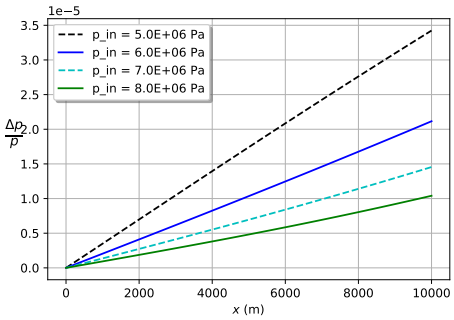

(a) Relative error of the pressure for several input pressures

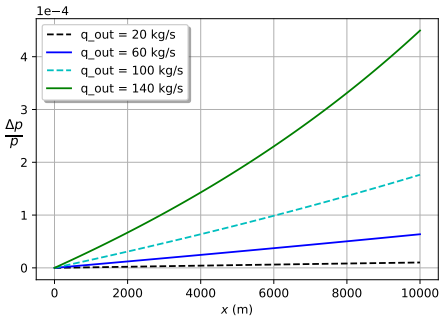

(b) Relative error of the pressure for several output flow rates

Figure 3.3: Comparison of the pressure profile for the isothermal Euler equations and the algebraic model for several input pressure and output flow rates

3.3. ALGEBRAIC MODEL

The Euler equations are given by a PDE involving partial derivatives with respect to space and time. The solution to this system will be transient, meaning that the variables involved will have certain dependency on time. On the other hand, the steady-state solution corresponds to the case in which the variables remain constant in time. This situation is of particular interest and it can be imposed by neglecting the partial derivatives with respect to time.

Despite the limitations of steady-state solutions, they have been widely used for the modeling of gas transport in pipes, particularly when the computational cost for solving systems of PDEs was large compared with the computational power. These steady-state solutions were originally formulated together with a specific friction factor, giving rise to the Weymouth equation for instance [5]. It is also possible to derive a steady-state solution from the isothermal Euler equations under certain assumptions, and it was demonstrated to generalize previously known steady-state laws [14].

The goal of this section is to derive a steady-state solution starting from the semilinear model. This will allow the comparison between all the models belonging to the model hierarchy. It will also allow to couple pipes described by transient and algebraic models, and this comparison is done in Chapter 5. Moreover, we will also be able to analyze the transient behavior when using hybrid models. This will be left for Chapter 6.

Although it is possible to particularize the isothermal Euler equations to steady-state regime by imposing the time derivatives equal to zero, the resulting ODE doesn't admit an analytical solution without further assumptions. However, it is possible to derive an algebraic model from the semilinear model.

After setting the time derivatives to zero the continuity equation (3.2a) simply becomes $\frac{\partial q}{\partial x} = 0$, meaning that the flow profile is constant throughout the pipe. For simplicity it will be assumed that the slope of the pipe is zero, so gravitational effects don't play a significant role. However, they could easily be included by assuming that the pressure

appearing in the term containing the gravitational effects can be set as an average pressure. After these simplifications, the semilinear model reduces to the ODE:

$$\frac{\partial p}{\partial x} = -\frac{RTz(p)}{2DA^2}\frac{q^2\lambda}{p} \tag{3.3}$$

In order to get an analytical solution to this equation, we also need to consider the compressibility factor as a constant, i.e., independent of the pressure. Assuming that the input pressure are known, the previous equation can be integrated for the entire pipe yielding the following relation between the flow and the input and output pressures:

$$q = \sqrt{\frac{2DA^2}{LRTz}}\frac{1}{\sqrt{\lambda}}\sqrt{p_1^2 - p_2^2} \tag{3.4}$$

A different formulation of this model can be obtained by integrating equation (3.3) for a given spatial coordinate x, obtaining the following spatial profile for the pressure:

$$p(x) = \sqrt{p_1^2 - \frac{RTz}{DA^2}\lambda q^2 (x - x_0)} \tag{3.5}$$

It is immediate to obtain expression (3.4) by particularizing equation (3.5) for $x = L$ and rearranging the resulting expression.

Figure (3.3) contains the relative errors between the pressure and flow profiles corresponding to the isothermal Euler equations and the algebraic model. The compressibility factor for the algebraic model has been computed as the average of the compressibility factor corresponding to the average pressure along the pipe. This is expected to introduce an additional source of error.

The relative error for the pressure profile for several input pressures behaves in a similar way as in the comparison between the isothermal and semilinear model. The relative error increases with the position and it is maximum for the smaller value of the input pressure. The maximum relative error observed corresponds to the pressure of $p_{in} = 5 \times 10^6 Pa$. For higher values the relative error decreases, being negligible for the highest pressure considered. The relative error for the flow rate remains with the same order of magnitude as for the comparison with the semilinear model.

In the case of different output flow rates, the relative error increases with the value of output flow rate, being the errors observed of the same order of magnitude as in the comparison between the isothermal Euler and semilinear equations. The fact that the error increases with the output flow rate can be justified with the same argument as for the semilinear model since the algebraic model has been proven to be the steady-state solution to the transient semilinear model. The relative error corresponding to the flow profile does not show a strong dependence with the output flow rate values and can be neglected.

From the previous discussion we can conclude that the algebraic model can be safely applied for the study of gas transport in pipelines in steady-state regime. Even though it is a very simple model it constitutes an accurate approximation of the pressure profile for a single pipe in steady-state regime. Moreover, the algebraic model is simple to

treat analytically and does not require the use of numerical techniques for obtaining the pressure profile.
In the present chapter we have been restricted to the analysis of isothermal models in a single pipe. It would be desirable to evaluate the suitability of both semilinear and algebraic models in more complicated networks involving the coupling of these models. This will be discussed in Chapter 5. Moreover, since the algebraic model has been derived as the steady-state solution of the semilinear model, it does not depend on time and it establishes an algebraic relation between the flow rate and pressure. Therefore it is expected that a change in time of one of the variables (pressure or flow rate or both) leads to an instantaneous change in the rest of the variables of the model. A transient analysis of the algebraic model becomes a topic of interest and it will be studied in Chapter 6.
Before proceeding any further, it becomes necessary to introduce the numerical methods used to solve the PDEs corresponding to the isothermal Euler equations and the semilinear model. This will be the focus of the next chapter.

4

NUMERICAL METHODS FOR SOLVING HYPERBOLIC PROBLEMS

The transient isothermal models presented in previous chapters constitute a system of PDEs, and in particular a hyperbolic problem. This type of problems are ubiquitous accross several disciplines and are used to describe a wide range of phenomena such as wave propagation and advective transport. The goal of this chapter is to introduce the mathematical background required for solving this type of differential equations along the methods commonly used. Special emphasis will be made in a particular method suitable for subsonic flow, and this will be the method used for the simulations of this study.

4.1. INTRODUCTION TO HYPERBOLIC PROBLEMS

The isothermal Euler equations in the previous chapter constitute a hyperbolic system of partial differential equations in space and time. Since only first order derivatives are present it is a system of first order partial differential equations. The structure of hyperbolic problems describing other phenomena like transport of chemical products is similar, allowing the study of these systems with techniques suitable for hyperbolic problems in general. If the number of dependent variables (the variables of interest, being pressure and flow rate in the case of gas transport) is more than one a hyperbolic system needs to be solved, and when there is only one variable it is called a hyperbolic scalar equation. This chapter will only consider hyperbolic systems, although the study of scalar equations provides with valuable insight for the study of more complex models. Consider a first order hyperbolic system in one dimension given by the equation:

$$u_t + f(u)_x = g(u) \tag{4.1}$$

where $u \in \mathbb{R}^m$ is the vector of unknowns, f is the so called flux function and g is the source term. A special case is when the right hand side of the equation (4.1) is zero. This homogeneous equation is known as a conservation law. The non-homogeneous

system is called a balance law. Each of those cases have their own particularities and these will be discussed in the following sections.

4.2. CONSERVATION LAWS

When the source term g in the right hand side of equation (4.1) is equal to zero, the following conservation law is obtained:

$$u_t + f(u)_x = 0 \tag{4.2}$$

This is the most general version of a conservation law in one dimension. Before proceeding any further, it is necessary to give a formal definition of hyperbolicity for systems of partial differential equations. The simplest case is when the system of equations is linear, given by the expression:

$$u_t + Au_x = 0 \tag{4.3}$$

where $A \in \mathbb{R}^{mxm}$ is a constant matrix. A linear system of the form (4.3) is called hyperbolic if the matrix A is diagonalizable with real eigenvalues. If this is the case the system can be decoupled into m independent equations and the solution of the original problem will be a combination of waves traveling at the characteritic speeds given by the eigenvalues of A. A nonlinear conservation law described by (4.2) is hyperbolic if the Jacobian $f'(u)$ of the flux function is diagonalizable with real eigenvalues for all physical values of u. This definition is closely related to the concept of characteristics. Moreover, for the problem being completely specified and guaranteeing existence and uniqueness it is necessary to include boundary and initial conditions.
It is easy to see that the isothermal Euler equations in (3.1) are not a conservation law since the system of equations is not homogeneous, containing terms responsible for gravity and friction effects. Indeed, the system (3.1) is a system of balance laws and will be discussed later in this chapter.

4.2.1. NUMERICAL METHODS FOR CONSERVATION LAWS

Due to their wide range of applications and their analytical intractability in most realistic cases, numerical methods for solving systems of conservation laws have been a subject of intensive research. One of the most common approaches is by Finite Volume Methods (FVM), based on the integral formulation of the conservation law.
For illustration purposes it is convenient to consider a simple scalar linear hyperbolic problem such as the advection equation. This model is used to describe transport of substances inside a fluid in one dimension, and it is given by:

$$u_t + \bar{v}u_x = 0 \tag{4.4}$$

where u represents the density of the substance and $\bar{v} > 0$ is the speed at which it is transported. From the FVM perspective, it is possible to derive the following scheme, also known as the upwind method:

$$u_i^{n+1} = u_i^n - \frac{\bar{v}\tau}{h}\left(u_i^n - u_{i-1}^n\right) \tag{4.5}$$

where τ is the time spacing, h the spatial lattice spacing and the indexes n and i correspond to the time and spatial indexes respectively. By rearranging the previous equation it is clear that it can be interpreted as a finite difference scheme backward in space and forward in time. The requirement for convergence of this numerical scheme serves to illustrate a more general feature of numerically solving hyperbolic problems, this being the Courant-Friedrichs–Lewy (CFL) condition. The CFL condition is a necessary condition that needs to be fulfilled when refining the lattice spacing for guaranteeing existence of a unique solution, and it ensures that the information is propagated at the correct speed. In particular, it states that a numerical method can be convergent only if its numerical domain of dependence contains the true domain of dependence of the PDE, at least in the limit as τ and h go to zero. This condition introduces the so called Courant number given by

$$\nu = \frac{\tau}{h} \max_p \left|\lambda^p\right| \tag{4.6}$$

and this number is needed to be $\nu \leq 1$. We will see that this requirement doesn't need to be satisfied by the numerical method that will be used for the simulations in this study.

4.3. BALANCE LAWS

Conservation laws are ubiquitous in science and engineering and achieve to describe the behavior of many physical problems. However, in most realistic situations the correct characterization of the system involves source terms. These terms are responsible of effects such as chemical reactions between the components or dissipative effects like friction. This will result in an additional term in the right hand side of a conservation law, yielding the following expression:

$$u_t + f(u)_x = g(u) \tag{4.7}$$

where g is a source term which depends on the variables of interest. In fact, the isothermal Euler equation containing friction and gravity terms are an example of a balance law. So far only methods for solving conservation laws have been discussed. The numerical treatment of balance laws is more complex, and the following subsection presents some insight on how to solve this type of problems.

4.3.1. NUMERICAL METHODS FOR BALANCE LAWS

A conceptually simple yet effective approach for solving systems of balance laws is the operator splitting method. This approach relies on the idea of separating the homogeneous and non homogeneous problems into two steps as follows:

$$A : u_t + f(u)_x = 0 \tag{4.8a}$$

$$B : u_t = g(u) \tag{4.8b}$$

The first step involves solving an homogeneous problem and this can be done with any of the available methods suitable for this, such as an upwind method. The second step

includes the non-homogeneity (source term) and constitutes an ODE that can also be solved with standard techniques.
In general it is expected that dividing the problem in this way introduces an splitting error which might compromise the accuracy and convergence of the solution. Another issue arises regarding the boundary conditions. The boundary conditions for the original equation (4.7) in general does not correspond to the boundary condition which needs to be applied to the homogeneous PDE (4.8b) corresponding to the first step of the method. For further details the reader is referred to Chapter 17 of [15]
It is clear that the numerical treatment of balance laws presents challenges which were absent for conservation laws at both convergence and implementation level. In the rest of this chapter we will focus on a method for solving systems of balance laws which is relatively simple to implement and circumvents some of the problems discussed in this chapter. In the case of the isothermal Euler equations the assumption made for this method is that the flow is subsonic, being the speed of the gas negligible in comparison with the speed of sound in the gas. Although this assumption seems restrictive at a first glance, most of the transient behavior in gas pipeline networks is restricted to the subsonic case.

4.4. IMPLICIT BOX SCHEME FOR SUBSONIC FLOW

The method presented in this section was published in [16] as a scheme suitable for large scale simulation of gas flow in pipelines. It relies on the weak formulation of the hyperbolic problem and it has been quickly adopted by the research community due to its relatively simple implementation compared with other traditional methods for systems of balance laws.
Consider a scalar first order hyperbolic problem in one dimension give by:

$$u_t + f(u)_x = g(u) \qquad (x,t) \in \mathbb{R} \times \mathbb{R}_+ \tag{4.9}$$

together with the initial condition denoted as:

$$u(x,0) = u_0(x) \qquad x \in \mathbb{R} \tag{4.10}$$

The proposed discretization scheme stems from the variational formulation of the equation (4.9), by multiplying this expression with a test function $\phi \in C_0^1(\mathbb{R} \times \mathbb{R}_+)$ and applying integration by parts, yielding:

$$\int_{-\infty}^{+\infty}\int_{0}^{+\infty}\left[u\phi_t + f(u)\phi_x\right]dtdx + \int_{-\infty}^{+\infty} u_0(x)\phi(x,0)\,dx = -\int_{-\infty}^{+\infty}\int_{0}^{+\infty} g(u)\phi dtdx \tag{4.11}$$

where $u \in L^\infty(\mathbb{R} \times \mathbb{R}_+)$. Assuming h and τ as the spatial and temporal lattice spacings, a box discretization of the domain as a box in space and time can be performed. The discretization proposed consists of the spatial interval $I_j = \left[\left(j-0.5\right)h, \left(j+0.5\right)h\right]$ and temporal interval $J_n = [n\tau, (n+1)\tau]$. These are cells constructed by central differences in space and backward differences in time respectively. The test function or ansatz is assumed to be a piecewise constant function of the form:

$$\bar{u}(x,t) = u_j^n \qquad (x,t) \in I_j \times J_n \tag{4.12}$$

where the solution has been approximated as $u_j^n \simeq u\left(jh, n\tau\right)$. The discretization scheme proposed can be written as:

$$\frac{u_{j-1}^{n+1} + u_j^{n+1}}{2} = \frac{u_{j-1}^n + u_j^n}{2} - \frac{\tau}{h}\left(f_j^{n+1} - f_{j-1}^{n+1}\right) + \tau \frac{g_{j-1}^{n+1} + g_j^{n+1}}{2} \tag{4.13}$$

where $f_j^n = f\left(u_j^n\right)$, $g_j^n = g\left(u_j^n\right)$ and the initial condition is given by $u_j^0 = \int_{I_j} u_0(x)\,dx$. It is worth noticing that this scheme is not explicit since the solution for a given timestep can not be obtained directly from the solution corresponding to the previous timestep. As a matter of fact, for obtaining the solution at any timestep a system of nonlinear equations need to be solved, resulting in an implicit method. Newton's method will be used for solving the system of nonlinear equations, and a brief introduction can be found in the next subsection of this chapter. The explicit expressions corresponding to the discretization of the isothermal Euler equations and the semilinear model will be left for Chapter 5.

The following lemma concerns the existence and uniqueness of the solution to the general balance law (4.7) under the discretization scheme (4.13):

Lemma 1 *[16] For $u^n \in L^1(\mathbb{Z})$, $f, g \in C^1(\mathbb{R})$, $g(0) = 0$, $g' \leq 0$, $f' \geq \lambda_{min} > 0$ and $\frac{\tau}{h} \geq \frac{1}{2\lambda_{min}}$, the scheme (4.13) admits a unique solution $u^{n+1} \in L^1(\mathbb{Z})$.*

It is worth mentioning that, although the condition contained in the previous lemma resembles the CFL condition, it prescribes quite the opposite. Given a certain lattice spacing, the CFL condition constitutes an upper bound for the timestep, meaning that the grid needs to be refined in time when is refined in space. On the other hand, the present scheme prescribes a lower bound for the time spacing, meaning that when the spatial lattice is refined, there is a limit for the refinement of the time spacing.

This is one of the most remarkable features of the discretization considered, as it allows to take larger timesteps as the grid is refined. This becomes particularly useful for reaching the steady state solution in a few timesteps in comparison with other methods. As a matter of fact, the steady state solution in the present study will be obtained by evolving an arbitrary initial state until reaching steady state. The stopping criterion will be the relative error between the solution between two consecutive time steps, which should remain above a certain predefined threshold.

Defining the variable $P = \frac{p}{z(p)}$ and gathering the variables P and q into the vector of unknowns $u = \begin{pmatrix} P \\ q \end{pmatrix}$ it is possible to express equations (5.7) as in (4.9). This constitutes a hyperbolic system since the eigenvalues of the Jacobian of the flux function f are real and given by $\sigma = v \pm c\left(p\right)$, where $c\left(p\right)$ is the speed of sound. In most practical applications of the transport equations the flow can be considered subsonic, where the speed of the gas is significantly lower than the speed of sound, $v << c$. In this situation the eigenvalues preserve their sign.

h	τ_{th}
25	0.329
50	0.164
100	0.082
200	0.041

Table 4.1: τ threshold value for several lattice spacings. Below this value the numerical method is expected to oscillate

τ	ν	oscillations
100	1.658×10^{1}	No
10	1.658	No
1	1.658×10^{-1}	No
0.1	1.658×10^{-2}	No
0.01	1.658×10^{-3}	Yes

(a) $h = 25$

τ	ν	oscillations
100	8.29	No
10	8.29×10^{-1}	No
1	8.29×10^{-2}	No
0.1	8.29×10^{-3}	No
0.01	8.29×10^{-4}	Yes

(b) $h = 50$

τ	ν	oscillations
100	4.145	No
10	4.145×10^{-1}	No
1	4.145×10^{-2}	No
0.1	4.145×10^{-3}	Yes
0.01	4.145×10^{-4}	Yes

(c) $h = 100$

τ	ν	oscillations
100	2.073	No
10	2.073×10^{-1}	No
1	2.073×10^{-2}	No
0.1	2.073×10^{-3}	Yes
0.01	2.073×10^{-4}	Yes

(d) $h = 200$

Table 4.2: Courant number and observation of oscillations as a function of τ for several lattice spacings

It is interesting to check if for a fixed lattice spacing h, instabilities arise for values of τ below the threshold value corresponding to the condition $\frac{\tau}{h} \geq \frac{1}{2\lambda_{min}}$. The case $\lambda_{min} = \min(v + c)$ has been chosen, although the same analysis applies to $\lambda_{min} = \min(|v - c|)$. For the boundary conditions in the simulations performed the velocity of the gas takes the value $v = 4.145$ m/s, being this value significantly smaller than the speed of sound and therefore being in subsonic regime. For this velocity $\frac{1}{2\lambda} = 1.644 \times 10^{-3}$ and the value for τ below which the numerical method becomes unstable can be computed. Table 4.1 shows this value for several lattice spacings, being the total length of the pipe $L = 5000$ m.

After computing this value the simulation of transient behavior of a perturbation in pressure was performed for several values of τ, both over and under the threshold of discussed previously. The results are shown in Table 4.2, where the Courant number ν and whether oscillations were observed have also been included. As the time step τ decreases, the Courant number decreases as well. It is observed that for high values of τ the Courant number is significantly higher than 1. No unstabilities were observed for $\tau > 1$ for any of the lattice spacings considered. However, when the value of τ was set

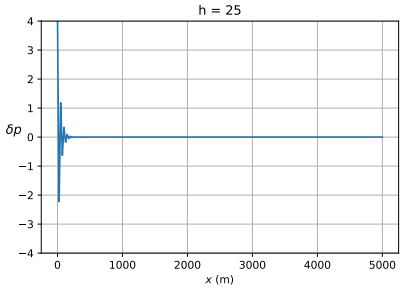

(a) $h = 25$

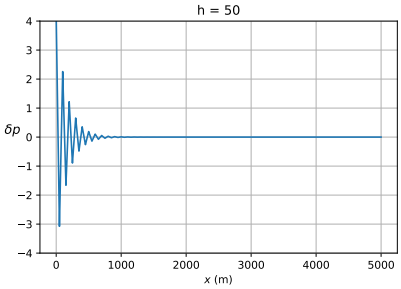

(b) $h = 50$

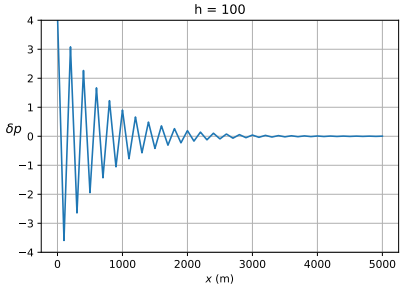

(c) $h = 100$

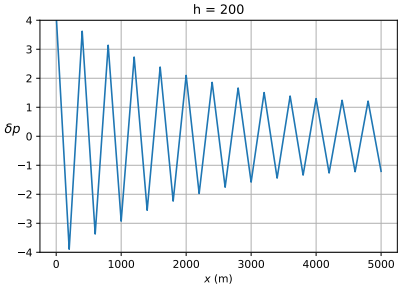

(d) $h = 200$

Figure 4.1: Oscillations for several lattice spacings with a fixed time step $\tau = 0.01$

below the threshold in Table 4.1, unstabilities can be observed. It is worth mentioning that even though the CFL condition is still fulfilled for all these values oscillations arise due to violating the condition $\frac{\tau}{h} \geq \frac{1}{2\lambda_{min}}$.
Figure 4.1 contains the pressure profile for the first time step for several lattice spacings with $\tau = 0.01$. The oscillations are clearly visible, and their spatial propagation seems to be higher the larger the lattice spacing as expected.

4.5. NEWTON'S METHOD

As discussed in the previous section, after the discretization of the Euler equations a nonlinear system of equations needs to be solved for each time step. Newton's method is one of the most well known procedures to solve this problem, and a brief discussion will be presented in the current section. A quite intuitive justification for Newton's method can be derived by Taylor expansion [17]. Given a set of nonlinear equations $F_l(x) = 0 \quad l = 1, \ldots, M$, a series expansion can be obtained around the given point x given a perturbation δx:

$$F_l(x + \delta x) = F_l(x) + \sum_i^M \frac{\partial F_l}{\partial x_i} \delta x_i + \mathcal{O}\left(\delta x^2\right) \tag{4.14}$$

Defining the Jacobian matrix as $J_{ij} = \frac{\partial F_i}{\partial x_j}$, the previous equation can be rewritten in a

more compact matrix notation as $F(x+\delta x) = F(x) + J.\delta x + \mathcal{O}\left(\delta x^2\right)$. Assuming that the perturbation is small enough, the quadratic and higher order terms can be neglected. Moreover, the condition $F(x+\delta x) = 0$ will be set. This simply means that the perturbation δx of interest is the required perturbation to solve the nonlinear system F. Therefore, the idea of the method is to 'search' for the solution following the direction of the perturbation. Under the aforementioned conditions, it is easy to obtain the relation

$$J.\delta x_k = -F \tag{4.15}$$

This constitutes a system of linear equations with unknown δx_k, and it can be efficiently solved by classical methods such as Gauss-Seidel elimination. The resulting iteration scheme is then given by:

$$x_{k+1} = x_k + \delta x_k \tag{4.16}$$

Newton's method is a particular case of a more general concept called simultaneous relaxation [18]. Under continuity conditions for F and non-singularity conditions for the Jacobian, Newton's method is proven to converge to the solution of the nonlinear system provided that the initial state is sufficiently close to the actual solution.
It is convenient to highlight some implementation details. The first step consists of defining symbolic variables for the pressure p and flow rate q, and then assembling the discretized PDE following scheme (4.13). The explicit expressions for the discretization of the equations corresponding to the models considered in this study can be found in Chapter 5, together with details on imposing boundary and coupling conditions. For Newton's method the Jacobian with respect to the discretized flow rate and pressure of the resulting nonlinear equations needs to be computed, and this will be done symbolically.
The system can then be initialized with numerical values. For obtaining the steady-state solution, the system can be initialized arbitrarily as long as the initialization satisfies the boundary and coupling conditions. The system will evolve in time, and the steady state is reached when the relative error between two consecutive time steps goes below a certain tolerance.

5

COUPLING OF ISOTHERMAL MODELS IN GAS PIPELINE NETWORKS

Transport of gas over long distances is usually carried out by gas pipeline networks. These structures often consist of tens or hundreds of elements, with pipes, valves and compressors being the most relevant ones. In this study we will only consider pipes. A pipeline network can be formulated as a directed finite graph $(\mathcal{J}, \mathcal{V})$, where $\mathcal{J}$ is the set of edges and $\mathcal{V}$ is the set of vertices [19]. Each edge $j \in \mathcal{J}$ corresponds to a pipe which, assuming that they are one dimensional, will be modeled by an interval $[a_j, b_j]$ denoting the initial and final position of the pipe. Each vertex $v \in \mathcal{V}$ corresponds to an intersection of pipes and, for a given vertex, the set of all indices of edges ingoing (outgoing) to the vertex v is denoted by $\delta_v^-(\delta_v^+)$.
In order to simulate the transport of gas in a pipeline network it becomes necessary to define coupling conditions for connected pipes. Given a node $v \in \mathcal{V}$ of the network, certain coupling conditions between the variables of the input δ_v^- and output pipes δ_v^+ need to be defined. In this study only isothermal models will be considered, namely the isothermal Euler equations, the semilinear and algebraic model. The dependent variables of the problem are the pressure p and mass-flow rate q, and the coupling conditions will concern these variables. The coupling conditions for connected pipes are expected to satisfy two requirements:

- The coupling conditions need to have a physical justification: Ideally the coupling between pipes will be supported by underlying physical laws concerning the behavior of the fluid at the intersection of pipes, such as conservation laws.
- The transport problem given the coupling conditions need to be well-posed: The coupling conditions need to guarantee existence and uniqueness of solutions to the transport problem.

The remainder of this chapter will be concerned with the coupling conditions when only a single model is used, as well as when different pipes are described by different models.

5.1. COUPLING CONDITIONS

From a physical perspective, there are three assumptions for the coupling of isothermal models at an intersection:

- There are no vacuum states present, meaning that the density ρ is always greater than zero. This assumption is expected to be fulfilled due to the conditions of operation of real gas networks.
- There is only one pressure at the intersection. Accurately modeling the real behavior of the pressure at an intersection might be cumbersome and not necessarily accurate, and therefore further simplifications are needed. Although having a single pressure at a given intersection might seem a strong assumption, this approximation has yielded accurate results in the modeling of gas networks and will be adopted.
- Mass flowing through an intersection is conserved: Unless there is a source or drain of flow at a given node, the incoming mass flow rate must be equal to the outgoing flow rate, meaning that the total mass is conserved. In the remaining of this study it will be assumed that no mass gets in or out at any inner node of the network.

These assumptions can be expressed formally as the following coupling conditions:

$$\rho_k > 0 \quad \forall k \in \delta_v^{\pm} \tag{5.1}$$

$$p\left(\rho_k(b_k-,t)\right) = p\left(\rho_{k'}(a_{k'}+,t)\right) \quad \forall k \in \delta_v^{-} \quad \forall k' \in \delta_v^{+} \tag{5.2}$$

$$\sum_{k\in\delta_v^-} q_k(b_k-,t) = \sum_{k\in\delta_v^+} q_k(a_k+,t) \tag{5.3}$$

A question of interest is the existence and uniqueness of solutions to the transport problem given these couplings. In case the solution exists, is unique and stable against perturbations in the data, the problem will be called well-posed, and it will be called ill-posed otherwise. Furthermore, two scenarios are possible:

- The transport in the entire network is described by a single model (the same model for all pipes): there are three different couplings in this scenario, namely isothermal Euler - isothermal Euler, semilinear - semilinear and algebraic - algebraic.
- The transport in different pipes is described by different models: In this case the coupling between different models need to be considered. There are three possibilities: Euler - semilinear, semilinear - algebraic and Euler - algebraic.

The well-posedness of the solution in the first case has been demonstrated in [20]. Moreover, it has also been demonstrated for the coupling of the isothermal Euler equations, semilinear and algebraic models [13]. Therefore the coupling conditions (5.1) guarantee the existence of an unique solution for the coupling of the isothermal models considered in this study.

5.2. MULTISCALE MODELING

Real gas networks can have hundreds of pipes and other elements. The isothermal Euler equations are a system of PDEs which is computationally expensive to solve, so if all the pipes of a gas network are modeled with a differential equation, the computational resources for solving the entire system might be quite large for realistic networks. However, for certain networks a fully detailed simulation is not even necessary. A better approach would be to use fine scale models such as the isothermal Euler equation and the semilinear model where high accuracy is desired, and coarse scale models such as the algebraic model where low accuracy can be tolerated. The goal of considering the coupling between different models is to allow for the hybrid modeling of the network. In particular the algebraic model is an analytical relation between the flow rate and pressure, meaning that no discretization of the variables is required and therefore the size of the problem diminishes significantly. Modeling a gas network with only the algebraic model is quite limited: it is a very simplistic steady state model, it doesn't consider any transient behavior of the gas and might not provide with accurate solutions in certain situations. However, with a hybrid modeling approach it could be possible to keep the balance between accuracy and computational complexity.

Assuming that the transport of each pipe of the network is described by different models, the entire set of pipes can be represented as $\mathcal{J} = \mathcal{J}_{Euler} \cup \mathcal{J}_{semi} \cup \mathcal{J}_{alg}$, where $\mathcal{J}_{Euler}$, $\mathcal{J}_{semi}$ and $\mathcal{J}_{alg}$ denote the set of pipes modeled with the isothermal Euler, semilinear and algebraic models respectively. The intersections between pipes will be considered as zero-dimensional domains (points in mathematical sense), and it is assumed that friction effects can be neglected at the intersection. Friction is present all along the pipes, but it is considered that there are no pressure losses inside the junction. Moreover, the pressure is supposed to be continuous as mentioned above. Therefore, an idealized and simple model for the intersections is assumed.

Once the coupling and boundary conditions are defined, it is necessary to impose these conditions. As discussed in Chapter 4 after discretizing the system of PDEs a system of non linear equations needs to be solved for each time step. The coupling and boundary conditions will be imposed by simply adding these constraints as algebraic equations to the system of nonlinear equations resulting from the discretization. This will be discussed in detail in the following sections.

5.3. Y-SHAPED NETWORK

In this section the coupling between the isothermal models discussed in Chapter 3 is considered for the Y-shaped network depicted in Figure 5.1. It is illustrative to present the hybrid modeling of the network in detail, including the different models governing transport in each pipe together with their discretization and the assembly of the result-

ing system of nonlinear equations. Although the Y-shaped network constitutes a simple network instance, its geometry allows to illustrate some key aspects for the study of more complex networks.

It is convenient to introduce the notation used. For the transient models the pipes will be discretized uniformly with equidistant spatial gridpoints $x_i = ih$, $i = 0, 1, \ldots, N_j$, being the number of spatial intervals $N_j = L_j/h$ where L_j is the length of pipe j. The temporal gridpoints will be denoted by t_k, $k = 0, 1, \ldots, M$, with uniform stepsize $\tau = \frac{T}{M}$ where T is the final time. The mass-flow rate and pressure at given spatial and temporal node will be denoted as $q^k_{j,i} := q_j(x_i, t_k)$ and $p^k_{j,i} := p_j(x_i, t_k)$.

The boundary conditions will be given by the input pressure p_{En} at the entry node and the output flow rates q_{Ex1} and q_{Ex2} at the exit nodes. The coupling conditions for the pressure and flow rate of the pipes at the intersections will be specified by equations (5.2) and (5.3) respectively. In the case of the Y-shaped network the continuity of pressure needs to be imposed on the pressure at the end of pipe 1 and at the beginning of pipes 2 and 3. Furthermore, the conservation of mass translates into the conservation of mass-flow rate at the inner node, and therefore the flow rate at the end of the input pipe 1 needs to be equal to the sum of the flow rates at the beginning of pipes 2 and 3. In order to fully specify the problem an initial state needs to be provided too. The boundary, coupling and initial state conditions can then be written as:

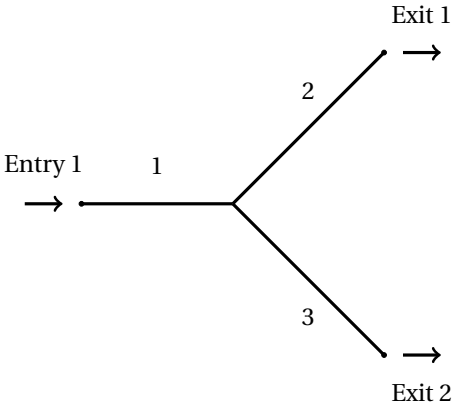

Figure 5.1: Y-shaped

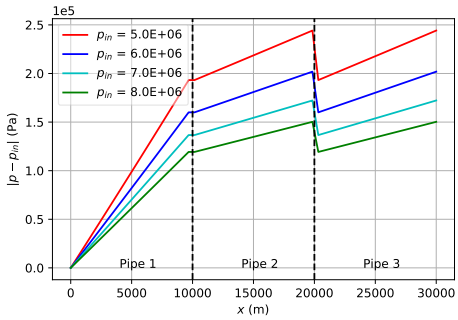

(a) Pressure drop for different input pressures

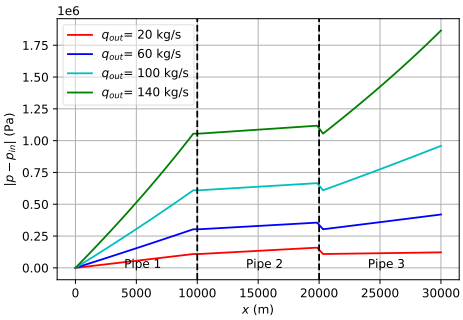

(b) Pressure drop for different output flow rates in pipe 3

Figure 5.2: Comparison of the pressure drop profile in the Y-shaped network for configuration $1,2,3 \in \mathcal{J}_{Euler}$

5

$$\begin{bmatrix} p_1(0,t) \\ q_2(L_2,t) \\ q_3(L_3,t) \end{bmatrix} = \begin{bmatrix} p_{En}(t) \\ q_{Ex1}(t) \\ q_{Ex2}(t) \end{bmatrix}, \tag{5.4}$$

$$\begin{bmatrix} p_1(L_1,t) \\ p_1(L_1,t) \\ q_1(L_1,t) \end{bmatrix} = \begin{bmatrix} p_2(0,t) \\ p_3(0,t) \\ q_2(0,t) + q_3(0,t) \end{bmatrix}, \tag{5.5}$$

$$\begin{bmatrix} q_j(x,0) \\ p_j(x,0) \end{bmatrix} = \begin{bmatrix} q_j^0(x) \\ p_j^0(x) \end{bmatrix}, \tag{5.6}$$

These conditions will remain independent of the models used, so they will be valid for the remainder of this section.
The parameters used in the simulations of this chapters are the same as in table 3.1. Moreover, several input pressure and output flow rates will be considered and indicated in the figures. The lattice and time spacing are set to $h = 100$ meters and $\tau = 10$ second respectively. Chen's friction factor is used and the compressibility factor for the algebraic model is computed as the average value of the compressibility factor for the isothermal Euler equations over the pipes.

5.3.1. EULER - EULER

Although we are mainly focused on the hybrid modeling of the network, it is convenient to consider a network modeled exclusively with the isothermal Euler equations. This will serve as a first step to illustrate how to couple pipes at the intersections, and will serve as a baseline for the subsequent hybrid models. Assuming that the three pipes of the Y-shaped network are modeled by the isothermal Euler equations, the network edges are given by $\mathcal{J} = \mathcal{J}_{Euler}$, and therefore the transport model for pipe j is given by:

$$\frac{\partial}{\partial t}\left(\frac{p_j}{RTz(p_j)}\right)+\frac{1}{A}\frac{\partial q_j}{\partial x}=0 \tag{5.7a}$$

$$\frac{1}{A}\frac{\partial q_j}{\partial t}+\frac{\partial p_j}{\partial x}+\frac{1}{A^2}\frac{\partial}{\partial x}\left(\frac{q_j^2 RTz(p_j)}{p_j}\right)=-\frac{gh'}{RT}\frac{p_j}{z(p_j)}-\frac{RT}{2DA^2}\frac{z(p_j)\,q_j|q_j|\lambda(|q_j|)}{p_j} \tag{5.7b}$$

Since the three pipes are modeled with the isothermal Euler equations, the expressions (5.7a) and (5.7b) are valid for j = 1,2,3. After discretizing the system (5.7) following the scheme given by (4.13), the resulting system of nonlinear equations can be written as:

$$F^k_{i+\sum_{\ell=1}^{j-1}N_\ell}=\frac{P^k_{j,i-1}+P^k_{j,i}}{2\tau}-\frac{P^{k-1}_{j,i-1}+P^{k-1}_{j,i}}{2\tau}+C\frac{q^k_{j,i}-q^k_{j,i-1}}{h}, \tag{5.8a}$$

$$\begin{aligned}F^k_{i+\sum_{\ell=1}^{j-1}N_\ell+\sum_{\ell=1}^{3}N_\ell}=&\frac{q^k_{j,i-1}+q^k_{j,i}}{2\tau}-\frac{q^{k-1}_{j,i-1}+q^{k-1}_{j,i}}{2\tau}+A\frac{p^k_{j,i}-p^k_{j,i-1}}{h}\\&+\frac{C}{h}\left(\frac{(q^k_{j,i})^2}{P^k_{j,i}}-\frac{(q^k_{j,i-1})^2}{P^k_{j,i-1}}\right)+\frac{gh'}{C}\frac{P^k_{j,i-1}+P^k_{j,i}}{2}\\&+\frac{C}{4D}\left(\frac{q^k_{j,i-1}|q^k_{j,i-1}|\lambda(|q^k_{j,i-1}|)}{P^k_{j,i-1}}+\frac{q^k_{j,i}|q^k_{j,i}|\lambda(|q^k_{j,i}|)}{P^k_{j,i}}\right),\end{aligned} \tag{5.8b}$$

$$F^k_{1+2\sum_{\ell=1}^{3}N_\ell}=q^k_{1,N_1}-q^k_{2,0}-q^k_{3,0}, \tag{5.8c}$$

$$F^k_{2+2\sum_{\ell=1}^{3}N_\ell}=p^k_{1,N_1}-p^k_{2,0}, \tag{5.8d}$$

$$F^k_{3+2\sum_{\ell=1}^{3}N_\ell}=p^k_{1,N_1}-p^k_{3,0}, \tag{5.8e}$$

$$F^k_{4+2\sum_{\ell=1}^{3}N_\ell}=q^k_{2,N_2}-q^k_{\mathrm{Ex1}}, \tag{5.8f}$$

$$F^k_{5+2\sum_{\ell=1}^{3}N_\ell}=q^k_{3,N_3}-q^k_{\mathrm{Ex2}}, \tag{5.8g}$$

$$F^k_{6+2\sum_{\ell=1}^{3}N_\ell}=p^k_{1,0}-p^k_{En}. \tag{5.8h}$$

for j = 1,2,3. The variable $P=\frac{p}{z(p)}$ and constant $C=\frac{RT}{A}$ have been defined for convenience. Equations (5.8a) and (5.8b) correspond to the discretized continuity and momentum equations respectively. On the other hand, the equations (5.8c) to (5.8h) correspond to the coupling and boundary conditions. It is clear that the system will be composed of partial differential equations together with algebraic constraints, being this better known as a differential algebraic equation (DAE) [19]. The coupling conditions relate the flow rates and pressures of the pipes at the intersection, and the boundary conditions impose the input values for the pressure and the output values for the flow rate.

Whereas the equations (5.8a) and (5.8b) describing the transport will be model dependent, the equations corresponding to the boundary and coupling conditions will re-

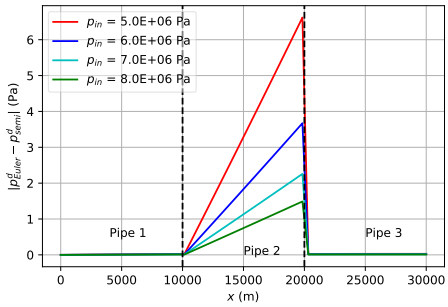

(a) Absolute error in pressure drop for different input pressures

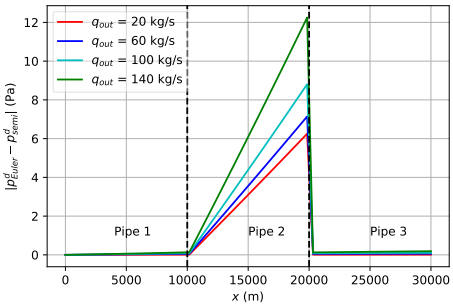

(b) Absolute error in pressure drop for different output flow rates in pipe 2

Figure 5.3: Comparison of the pressure drop profile in the Y-shaped network for configurations $1,2,3 \in \mathcal{J}_{Euler}$ and $1,3 \in \mathcal{J}_{Euler}, 2 \in \mathcal{J}_{semi}$

5

main the same for different configurations of transport models. It is also worth mentioning that it is necessary to carefully keep track of the indexes of each nonlinear equations for the correct assembly of the system. The indexing will vary depending on the choice of the models for each pipe, this being explicitly shown in the following subsections.

The main quantity of interest is the pressure drop along the pipes. The pressure drop is defined as the absolute value of the difference between the input pressure and the pressure profile, $p^d = |p_{in} - p|$. Figure 5.2 shows the pressure drop for configuration $1,2,3 \in \mathcal{J}_{Euler}$ for the Y-shaped network for several input pressures and output flow rates in pipe 3. In case of variable input pressure it is observed that the pressure drop is one order of magnitude smaller than the input pressure and that it decreases when the input pressure increases. In case of variable output flow rate the pressure drop is of the same order of magnitude as the input pressure and it decreases with the output flow. In the following subsections a comparison of the pressure drop between hybrid models using the semilinear and algebraic models is done.

5.3.2. EULER - SEMILINEAR

Both the isothermal Euler equations and the semilinear model are transient models, and therefore described by a system of PDEs. The only difference between these two models is that the quadratic term with the flow rate in the momentum equation is neglected in the semilinear model. Assuming that the network is modeled using the isothermal and semilinear equations, the edges of the network graph can be expressed as $\mathcal{J} = \mathcal{J}_{Euler} \cup \mathcal{J}_{semi}$. In the particular case of the Y-shaped network, pipes 1 and 3 are assumed to follow the isothermal Euler equations, and pipe 2 the semilinear model, so $1,3 \in \mathcal{J}_{Euler}$ and $2 \in \mathcal{J}_{semi}$.

Since both isothermal and semilinear contain the continuity equation (which remains the same for these two models), equation (5.7a) will be valid for $j = 1,2,3$. The momentum equation differs, however, and therefore equation (5.7b) is valid for $j = 1,3$, and the

momentum equation for $j = 2$ will be given by:

$$\frac{1}{A}\frac{\partial q_j}{\partial t} + \frac{\partial p_j}{\partial x} = -\frac{gh'}{RT}\frac{p_j}{z(p_j)} - \frac{RT}{2DA^2}\frac{z(p_j)\,q_j\,|q_j|\,\lambda(|q_j|)}{p_j} \tag{5.9}$$

and after applying the discretization (4.13) the corresponding set of nonlinear equations for pipe 2 is given by:

$$\begin{aligned} F^k_{i+\sum_{\ell=1}^{2} N_\ell + \sum_{\ell=1}^{3} N_\ell} = {} & \frac{q^k_{j,i-1} + q^k_{j,i}}{2\tau} - \frac{q^{k-1}_{j,i-1} + q^{k-1}_{j,i}}{2\tau} + A\frac{p^k_{j,i} - p^k_{j,i-1}}{h} \\ & + \frac{gh'}{C}\frac{P^k_{j,i-1} + P^k_{j,i}}{2} \\ & + \frac{C}{4D}\left(\frac{q^k_{j,i-1}|q^k_{j,i-1}|\lambda(|q^k_{j,i-1}|)}{P^k_{j,i-1}} + \frac{q^k_{j,i}|q^k_{j,i}|\lambda(|q^k_{j,i}|)}{P^k_{j,i}}\right), \end{aligned} \tag{5.10a}$$

5

The full network will be described by the continuity equation (5.8a) for j = 1,2,3, and by the momentum equations (5.8b) for j = 1,3 and (5.10a) for j = 2.
Figure 5.3 contains the absolute error of the pressure drop profiles for configurations $1,2,3 \in \mathcal{J}_{Euler}$ and $1,3 \in \mathcal{J}_{Euler}, 2 \in \mathcal{J}_{semi}$. As expected, the largest error is observed in the pipe described by the semilinear model, being the error in the pipes modeled with the isothermal Euler equations significantly smaller. It is also observed that the error is inversely proportional to the input pressure and directly proportional to the output flow rate.
The error in pressure grows along the pipe, and this can be justified by two reasons; the pressure has a free boundary condition at the output node. Moreover, the higher the pressure the bigger the difference between the isothermal Euler equations and the semilinear model due to the aforementioned quadratic term.
From a qualitative perspective, modeling pipe 2 with the semilinear model does not affect significantly the pressure profile on pipe 3. This is due to the similarity between the isothermal Euler equations and the semilinear model, being both transient models. Although the flow rate is specified as a boundary condition at the output nodes, this condition has roughly the same effect for both the isothermal Euler equations and the semilinear model, and therefore there are no significant differences between these two configurations. In the next subsection it will be demonstrated that modeling pipe 2 with the algebraic model will affect the error in pressure drop to a greater extent.
It can be concluded that for this configuration the steady-state solution with the full network modeled with the isothermal Euler equations and the hybrid model with the semilinear model are equivalent.

5.3.3. EULER - ALGEBRAIC

In this case the edges of the network are given by $\mathcal{J} = \mathcal{J}_{Euler} \cup \mathcal{J}_{alg}$. As before, pipes 1 and 3 will be modeled with the isothermal Euler equations, $j = 1,3 \in \mathcal{J}_{Euler}$. Pipe 2 will be governed by the algebraic model, and therefore $j = 2 \in \mathcal{J}_{alg}$. The algebraic model for pipe 2 can be written as:

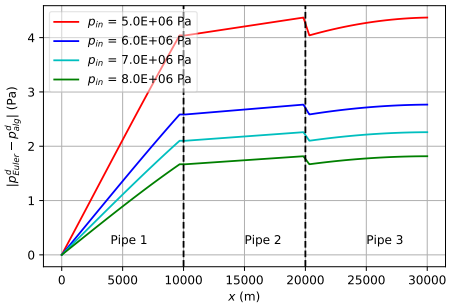

(a) Absolute error in pressure drop for different input pressures

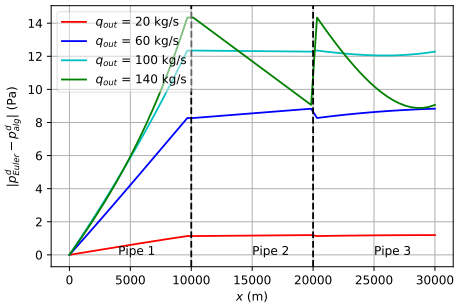

(b) Absolute error in pressure drop for different output flow rates in pipe 2

Figure 5.4: Comparison of the pressure drop profile in the Y-shaped network for configurations $1,2,3 \in \mathcal{J}_{Euler}$ and $1,3 \in \mathcal{J}_{Euler}, 2 \in \mathcal{J}_{alg}$

5

$$p_j^2(L_j,t) = p_j^2(0,t) - \frac{RTz(\bar{p}_j)}{DA^2} L_j \lambda(|q_j(t)|) q_j^2(t) \tag{5.11}$$

The equations corresponding to pipes modeled with the algebraic model don't need to be discretized. These equations will be included as non linear equations as:

$$F^k_{1+\sum_{\ell=1}^{2} N_\ell} = \left(p^k_{j,N_j}\right)^2 - \left(p^k_{j,0}\right)^2 + \frac{RTz}{DA^2} L_j \lambda\left(\left|q^k_{j,0}\right|\right)\left(q^k_{j,0}\right)^2 \tag{5.12}$$

The full network model will be specified by equations (5.8a) and (5.8b) for $j = 1,3$ and the algebraic equation (5.12) for $j = 2$.

Figure 5.4 shows the absolute error for the pressure drop between configurations $1,2,3 \in \mathcal{J}_{Euler}$ and $1,3 \in \mathcal{J}_{Euler}, 2 \in \mathcal{J}_{alg}$. As before, the error decreases when increasing the input pressure, and decreases when decreasing the output flow rate. It is observed that in this case the order of magnitude of the error in pipes 2 and 3 is the same and they exhibit similar behavior. The continuity of the error for the pressure drop can be observed well in this configuration, this being a consequence of the continuity condition imposed to the pressure at the junction as a coupling condition.

The algebraic model seems to have a more significant effect in the network than the semilinear model. We can interpret this result as follows: the algebraic model assumes that the flow rate is constant along the pipe, and therefore the flow rate in the algebraic pipe will be equal to the output flow rate since this is an output pipe. This affects the value of the flow rate on pipes 1 and 3 at the junction. Since pipe 3 is an output pipe, the flow rate at the end will be equal to the output flow rate. Therefore by modeling pipe 2 with the algebraic model the boundary condition regarding the output flow rate is 'extended' to the junction node since the flow rate is constant. This will modify the flow profile in pipe 3 more than when the semilinear model was used. Moreover, since the semilinear and algebraic model are equivalent in steady-state regime, they exhibit

roughly the same pressure profile in this configuration. It also modifies significantly the pressure profile in pipe 1, more than when the semilinear model was used.
In conclusion, using the semilinear and algebraic models yield similar results for the steady-state solution of the network considered. However, it was observed that using the algebraic model alters the pressure profile in a more significant way than using the semilinear model. This will become evident in the transient analysis in Chapter 6.

5.4. THREE PIPES

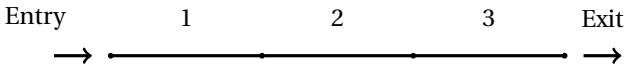

Figure 5.5: three pipes

In the case of the Y-shaped network the pipe modeled with the semilinear and algebraic model was an output pipe. It also becomes interesting to study the case in which the pipe described by the semilinear or algebraic model is an inner pipe. A simple case is a network composed by three pipes in series as depicted in Figure 5.5. This benchmark network was also studied in [13]. We are interested in the error between the pressure drop profiles when the entire network is modeled with the isothermal Euler equations and when pipe 2 is described by the semilinear and algebraic model.
The parameters used in the simulations of the three pipe network are the same as for the Y-shaped network, as well as the friction and compressibility factor.

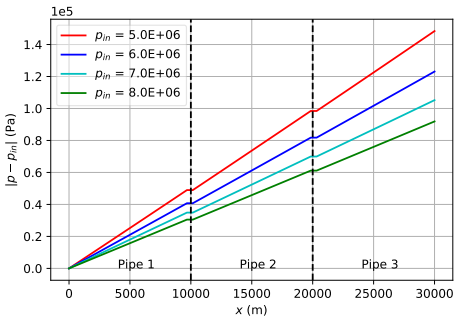

(a) Pressure drop profile for different input pressures

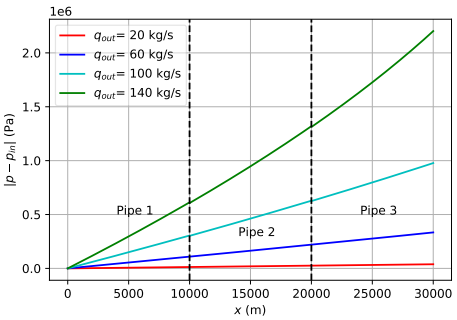

(b) Pressure drop profile for different output flow rates in pipe 3

Figure 5.6: Pressure drop profile in the three pipes network for configuration $1,2,3 \in \mathscr{J}_{Euler}$

Figure 5.6 contains the pressure drop profiles for the three pipe network for several values of input pressure and output flow rates for configuration $1,2,3 \in \mathscr{J}_{Euler}$. It is observed that the pressure drop decreases when the input pressure increases and that the drop decreases with the output flow rate, as with the Y-shaped network. Since the network considered consists in three pipes connected in series, the continuity of pressure at the intersections is observed.

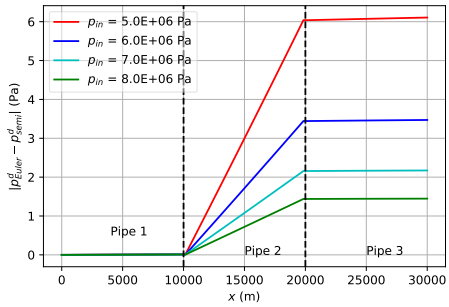

(a) Absolute error in pressure drop for different input pressures

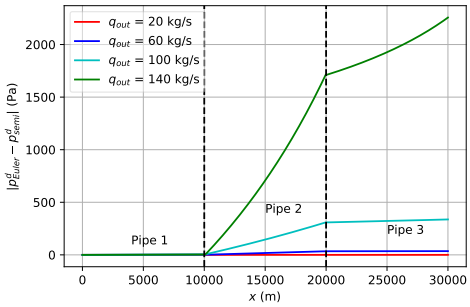

(b) Absolute error in pressure drop for different output flow rates in pipe 3

Figure 5.7: Comparison of the pressure drop profile in the three pipes network for configurations $1,2,3 \in \mathcal{J}_{Euler}$ and $1,3 \in \mathcal{J}_{Euler}, 2 \in \mathcal{J}_{semi}$

Figure 5.7 shows the absolute error of the pressure drop profile between configurations $j = 1,2,3 \in \mathcal{J}_{Euler}$ and $j = 1,3 \in \mathcal{J}_{Euler}$, $j = 2 \in \mathcal{J}_{semi}$ for different input pressures and output flow rates. As before the error in pressure drop is inversely proportional to the input pressure and inversely proportional to the output flow rate. Moreover, the continuity condition for the pressure is fulfilled at the junctions. The results in this plot are quite similar to the corresponding to configurations $j = 1,2,3 \in \mathcal{J}_{Euler}$ and $j = 1,3 \in \mathcal{J}_{Euler}$, $j = 2 \in \mathcal{J}_{alg}$ in Figure 5.8.

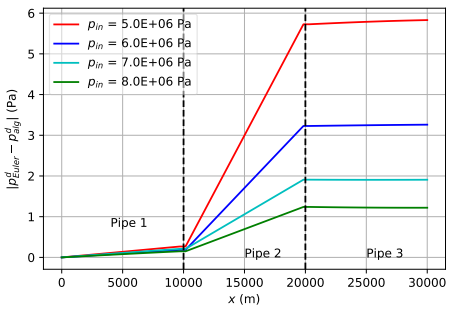

(a) Absolute error in pressure drop for different input pressures

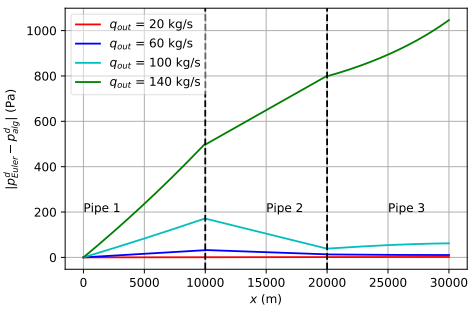

(b) Absolute error in pressure drop for different output flow rates

Figure 5.8: Comparison of the pressure drop profile in the three pipes network for configurations $1,2,3 \in \mathcal{J}_{Euler}$ and $1,3 \in \mathcal{J}_{Euler}, 2 \in \mathcal{J}_{alg}$

It is noted that the difference in pressure drop for high values of flow rate is several orders of magnitude higher than for low values of flow rate. This indicates that for high output flow rates the semilinear and algebraic models might differ significantly from the isothermal Euler. This was already discussed in Chapter 3. When considering vari-

able output flow rates, the difference in pressure drop between the different configurations is greater than for the Y-shaped network.
Although the network considered doesn't offer as interesting phenomenology as the Y shaped network for steady state, it will be used in Chapter 6 for the transient analysis when coupling different models. It will be demonstrated that it exhibit interesting behavior when considering pipe 2 with algebraic model in transient regime.
From the analysis in this chapter it can be concluded that networks described by hybrid models belonging to the isothermal model hierarchy yield equivalent results in steady-state regime. Moreover, the results for the benchmarks networks indicate that there exist substantial differences between using the semilinear and algebraic models. Even though they are demonstrated to be the same model in steady-state conditions, the algebraic model affects the overall pressure profile of the network more significantly due to the assumption of constant flow rate along the pipe. These differences will become more evident in the transient analysis of Chapter 6.

6

TRANSIENT ANALYSIS

Transient behavior of gas pipeline networks is a topic of interest in gas networks research. In practical situations the supply and demand of gas will change over time and therefore a transient analysis becomes necessary for modeling the time dependent behavior of the network. Moreover, transient behavior might be important for other purposes such as leakage detection.
Although so far the focus of this study has been the steady-state solution to the transport problem, the isothermal Euler equations and semilinear models are in fact time-dependent models. On the other hand, the algebraic model constitutes a steady-state solution and does not involve time derivatives. If the algebraic model is used for modeling some of the pipes of the network, interesting phenomenology is expected to arise. In particular, since the pressure and mass-flow rate are related by an algebraic relation, any perturbation in one of the variables will translate in an instantaneous perturbation of the rest of variables. Of special interest is the study of networks where both transient and algebraic models are used. The instantaneous propagation of the perturbations in the algebraic model is expected to affect the pressure and flow rate of the pipes connected to the algebraic pipe. This would be equivalent to have a model with a infinite speed of sound in the algebraic pipes, and this is expected to affect significantly the overall behavior of the network.
It would be desirable then to compare the behavior of the hybrid network with respect to a network using only the semilinear model. Moreover, it would also be of interest to derive analytical solutions when possible. These two will be the focus of this chapter.

6.1. TRANSIENT OF SEMILINEAR MODEL

The isothermal Euler equations (3.1) don't admit analytical solutions due to the nonlinearity of the terms involved and due to the source terms. In this study it has been demonstrated that the semilinear model constitutes a good approximation to the isothermal Euler equations for high values of pressure. Moreover, in this model the nonlinear term in the momentum equation is neglected. If we consider the case without friction, the resulting model is given by:

$$\frac{1}{RTz}\frac{\partial p}{\partial t}+\frac{1}{A}\frac{\partial q}{\partial x}=0 \tag{6.1a}$$

$$\frac{1}{A}\frac{\partial q}{\partial t}+\frac{\partial p}{\partial x}=0 \tag{6.1b}$$

Assuming that the compressibility factor doesn't depend on the pressure, this model is linear and analytically tractable. Taking the partial derivatives with respect to t in equation (6.1a),the partial derivative with respect to x in equation (6.1b) and equating the resulting terms $\frac{\partial^2 q}{\partial t \partial x}$ we obtain:

$$\frac{\partial^2 p}{\partial t^2}=c^2\frac{\partial^2 p}{\partial x^2} \tag{6.2}$$

where $c=\sqrt{RTz}$ is the speed of sound, which depends on the properties of the gas as well as on the temperature. This is the wave equation for the pressure. The wave equation for the mass-flow rate can be obtained in an analogous way. The wave equation admits a family of solutions of the form $f(x\pm ct)$. For analytical tractability a harmonic solution for the pressure and flow rate will be considered, being given by:

$$p(x,t)=p_0 e^{i(\omega t-kx)} \tag{6.3a}$$

$$q(x,t)=q_0 e^{i(\omega t-kx)} \tag{6.3b}$$

where p_0 and q_0 are the pressure and flow rate amplitudes, ω is the angular frequency and k is the wave number. Substituting the ansatz (6.3a) in the expression $\frac{1}{A}\frac{\partial q}{\partial t}+\frac{\partial p}{\partial x}=0$ the following relation between the time dependent values for flow rate and pressure can be derived:

$$q=A\frac{k}{\omega}p=\frac{A}{c}p \tag{6.4}$$

where the expression $c=\frac{\omega}{k}$ for a plane wave has been used. It is worth mentioning that this solution is only valid for non dissipative transport. An analytical treatment of the transient behavior of the semilinear model considering friction effects will be left for later in this chapter.

6.1.1. REFLECTION AND TRANSMISSION COEFFICIENTS

As mentioned earlier the boundary conditions imposed at the input nodes is the input pressure, whereas at the output nodes the mass-flow rate is specified as the boundary conditions. Therefore, the output pressure is a degree of freedom and does not have any condition imposed at the end of the pipe, whereas the output flow rate is fixed. This distinction is expected to yield different phenomenology for the pressure and flow profiles at the output nodes.

For studying the behavior of the system at the output nodes it is convenient to consider the boundary node as the intersection between two pipes. The first pipe will correspond to the real pipe considered, and the second pipe of the intersection will represent a fictitious pipe. It is assumed that the two pipes of the junction have different

speeds of sound, and therefore the behavior of the system will be described by the two wave equations, one corresponding to each pipe:

$$\frac{\partial^2 u_i}{\partial t^2} = c_i^2 \frac{\partial^2 u_i}{\partial x^2} \tag{6.5}$$

In a general situation, an incoming wave will travel in the input pipe with positive speed. Once this wave reaches the end of the pipe part of the incoming wave will be reflected and part of it will be transmitted to the second pipe. This scenario allows for the computation of the transmission and reflection coefficients at an intersection [21].
Denoting the incident wave as u_I, the reflected wave as u_R and the transmitted wave as u_2, the solution in the first and second pipe will be given by:

$$u_1(x,t) = u_I\left(t - \frac{x}{c_1}\right) + u_R\left(t + \frac{x}{c_1}\right) \tag{6.6a}$$

$$u_2(x,t) = u_2\left(t - \frac{x}{c_2}\right) \tag{6.6b}$$

It is expected that the reflected and transmitted wave depend on the incoming wave, so the reflected and transmitted wave can be expressed in terms of the incoming wave. Further conditions need to be imposed, namely continuity conditions involving the solution for both pipes, as well as the continuity for the first derivative:

$$u_1(0,t) = u_2(0,t) \tag{6.7a}$$

$$\left.\frac{\partial u_1}{\partial x}\right|_{x=0} = \left.\frac{\partial u_2}{\partial x}\right|_{x=0} \tag{6.7b}$$

Imposing these conditions in equations (6.6a) and (6.6b) and rearranging the resulting terms the expressions for the reflected and transmitted waves at the intersection can be written as:

$$u_R(t) = \mathscr{R} u_I(t) \tag{6.8a}$$

$$u_2(t) = \mathscr{T} u_I(t) \tag{6.8b}$$

where $\mathscr{R} = \frac{c_2 - c_1}{c_1 + c_2}$ and $\mathscr{T} = \frac{2c_2}{c_1 + c_2}$ are the reflection and transmission coefficients respectively. It is noticeable that these coefficients only depend on the propagation speeds of each pipe.
The aforementioned analysis can be applied to both flow rate and pressure separately. Assuming that the flow rate is the variable of interest, $u_i = q_i$. Since the value of the flow at the boundary is fixed, the boundary condition is considered as a hard boundary condition. In this case the second pipe won't be affected by the incoming wave at all since the flow rate at the boundary node does not change. This is equivalent to the second pipe having a propagation speed of zero, i.e, $c_2 = 0$. Imposing this value in the reflection and transmission coefficients we obtain $\mathscr{R} = -1$ and $\mathscr{T} = 0$ respectively.

This means that all the incoming wave will be completely reflected, and the negative sign means that the amplitude of the reflected wave will have the opposite sign of the incoming amplitude. On the other hand, there won't be any transmitted wave as expected.

In the case of pressure $u_i = p_i$. The pressure is not fixed at the boundary and therefore its behavior is expected to differ from the flow rate. Since there is no condition on the pressure it can be assumed that the propagation speed in the second pipe is infinite, $c_2 = +\infty$. Taking this limit in the expressions for the reflection and transmission coefficients it is easy to obtain $\mathscr{R} = 1$ and $\mathscr{T} = 2$. The reflected wave is this case preserves the sign of the incoming wave. The transmission coefficient indicates that the amplitude of the transmitted wave will be twice the amplitude of the incoming wave. Although in reality there won't be a second pipe, this effect will be noticeable at the boundary itself, the value of the pressure at the boundary increasing to twice the amplitude of the incoming wave and then being reflected without a change of sign.

In this section we have only focused on the behavior of a single pipe at its output node. The reflection and transmission at the input node can be treated in an analogous way by considering the pressure fixed (hard boundary) and no conditions on the flow rate (soft boundary). In this case a reflection with change of sign is expected for the pressure and a reflection preserving the sign for the flow.

The calculation of transmission and reflection coefficients can also be applied to more complex junctions. In particular, it is of special interest to derive transmission and reflection coefficients for the Y-shaped network, and this will be done during the analysis of the transient behavior without friction in section 6.3.

6.2. PERTURBATION ANALYSIS OF STEADY-STATE MODEL

It has been proven that the algebraic model constitutes the steady-state solution to the semilinear model. Due to its algebraic nature and to the lack of transient components, any time-dependent perturbation of the terms involved will instantaneously translate into time-dependent perturbations for the rest of variables. The variables considered relevant for transport are the mass-flow rate, the input and the output pressure. The mass-flow rate is considered constant along the pipe. The output pressure is in general smaller than the input pressure due to friction effects, the mass-flow rate together with the friction factor determining the value of the output pressure.

In a practical situation a pipe described by the algebraic model will be connected to a pipe described by a transient model. A perturbation propagating in the transient pipe will reach the algebraic pipe, being this perturbation both in pressure and flow rate. It becomes interesting to study the effects of an incoming perturbation in the value of the output pressure. The pressure profile for the algebraic model is given by:

$$p(x,t) = \sqrt{p_1^2(t) - \frac{RTz}{DA^2}\lambda q^2(t)(x - x_0)} \tag{6.9}$$

For simplicity the constant $\alpha = \frac{RTz}{DA^2}\lambda L$ will be used. With this notation the pressure at the output node of the pipe will be given by the expression:

$$p(L,t) = \sqrt{p_1^2(t) - \alpha q^2(t)} \tag{6.10}$$

where the input pressure and flow rate along the pipe are considered as time-dependent quantities. The initial state will be the steady-state solution, specified by the input pressure p_{10}, the constant flow rate q_0 and the steady-state output pressure denoted as:

$$p(L,0) = \sqrt{p_1^2(0) - \alpha q^2(0)} = \sqrt{p_{10}^2 - \alpha q_0^2} \equiv p_{20} \tag{6.11}$$

A simple approach is to assume a small perturbation in the input pressure given a steady-state solution. The time-dependent input pressure given a steady-state solution is given by:

$$p_1(t) = p_{10} + \delta p(t) \tag{6.12}$$

where $\delta p(t)$ is a small perturbation which fulfills $\delta p(0) = 0$ and $\frac{\delta p(t)}{p_{10}} \ll 1$. The perturbation is assumed small enough that only first order terms containing it will be considered. This allows to linearize the second order terms arising from the quadratic term in equation (6.10):

$$p_1^2(t) = \left(p_{10} + \delta p(t)\right)^2 \simeq p_{10}^2 + 2p_{10}\delta p(t) \tag{6.13}$$

In a realistic scenario perturbations in both input pressure and flow rate will be present. However, for illustrative purposes it is convenient to study the effects of perturbations in each of these variables separately.

6.2.1. PERTURBATION IN PRESSURE

In this subsection the flow rate along the pipe will be assumed constant in time and only a perturbation in the input pressure will be considered. In this scenario the exact time-dependent output pressure can be written as:

$$p(L,t) = \sqrt{p_1^2(t) - \alpha q_0^2} \tag{6.14}$$

Substituting expression (6.12) in (6.14) and making use of the definition of the steady-state output pressure the exact pressure at the output node is given by the expression:

$$p(L,t) = p_{20}\sqrt{1 + 2\frac{p_{10}}{p_{20}^2}\delta p(t)} \tag{6.15}$$

Since the perturbation is small compared with the steady-state solution it is safe to assume that the second term inside the square root is small compared to 1, and therefore the previous expression can be linearized by performing a Taylor expansion. The resulting approximation for the output pressure is then given by:

$$p(L,t) \simeq p_{20}\left(1 + \frac{p_{10}}{p_{20}^2}\delta p(t)\right) = p_{20} + \frac{p_{10}}{p_{20}}\delta p(t) \tag{6.16}$$

The previous expression indicates that the pressure at the output is equal to the steady-state output pressure plus a term which depends linearly with the perturbation in the

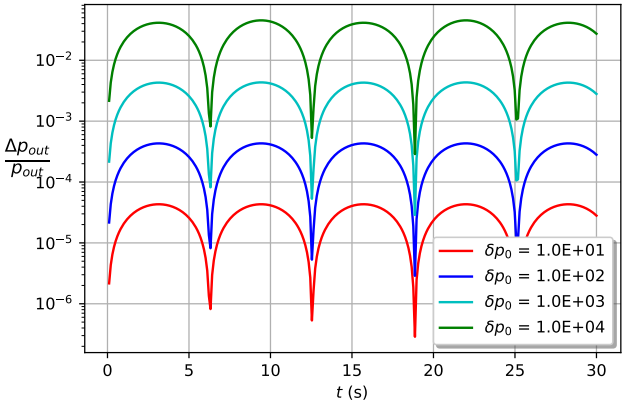

Figure 6.1: Relative error between the exact output pressure (6.10) and the first order approximation given by (6.16)

input pressure. Therefore, the response of the algebraic model to small perturbations in the input pressure is linear with a slope equal to the quotient of the steady-state pressures at the input and output nodes. Since the output steady pressure is always smaller than the input steady pressure due to friction effects, the coefficient joining the perturbation will always be greater than one. This suggests that the pressure at the output node will be greater that at the input, being amplified by the aforementioned quotient. However, for realistic values of the friction coefficient this quotient will be close to one, and therefore the magnitude of the perturbation at the output will be roughly equal to the magnitude of the pressure at the input.

In order to check the accuracy of the approximation, a comparison between the exact value and the first order approximation is presented in Figure 6.1. The chosen time dependent perturbation is given by $\delta p(t) = \delta p_0 \sin(0.5t)$ where δp_0 is the amplitude of the perturbation. The parameters in table 3.1 are used, the length of the pipe is $L = 10000$ meters, the compressibility factor is assumed $z = 1$ and a friction factor of $\lambda = 0.5$ is chosen. For these parameters the output pressure takes the value $p_{20} = 752441$ Pa. Although the value for the friction factor is very large for being realistic, it has been chosen to achieve a relatively large slope in the linear respose of the algebraic model (6.16). The comparison has been made for different amplitudes in order to observe the goodness of the approximation. There is good agreement between the exact and the approximate output pressure. It is evident that the relative error increases with the amplitude, something expected since the linear approximation relies on the fact that the perturbation is small compared to the steady state pressure.

6.2.2. PERTURBATION IN FLOW RATE AND PRESSURE

Assuming a steady-state flow rate denoted by q_0 a perturbation around this value is considered. The time-dependent constant flow rate along the pipe is then given by the

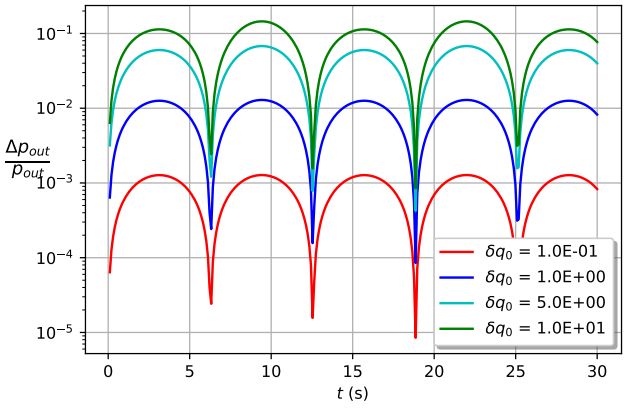

Figure 6.2: Relative error between the exact output pressure (6.10) and the first order approximation given by (6.19) keeping the input pressure constant

expression:

$$q(t) = q_0 + \delta q(t) \tag{6.17}$$

where $\delta q(t)$ is the perturbation in flow with $\delta q(0) = 0$ and $\frac{\delta q(t)}{q_0} \ll 1$. As with the pressure, second order terms will be neglected. Substituting expression (6.17) in equation (6.10) and using the definition of the steady-state pressure at the output node, the output pressure can be expressed as:

$$p(L,t) = p_{20}\sqrt{1 + \frac{2p_{10}}{p_{20}^2}\delta p(t) - \frac{2\alpha q_0}{p_{20}^2}\delta q(t)} \tag{6.18}$$

Assuming that the two terms proportional to the perturbations in flow rate and pressure are small, the previous expression can be linearized by a Taylor expansion, yielding the value for the output pressure:

$$p(L,t) \simeq p_{20} + \frac{p_{10}}{p_{20}}\delta p(t) - \frac{\alpha q_0}{p_{20}}\delta q(t) \tag{6.19}$$

The resulting expression suggests that for small perturbations the response of the algebraic model is linear with the perturbations in input pressure and flow rate. The negative sign of the term corresponding to the flow rate indicates that the output pressure will decrease when the flow increases. This is the expected behavior since the friction term is directly proportional to the flow rate and this causes a larger pressure loss along the pipe when the flow is increased.
Figure 6.2 shows the relative error between the exact and the first order solution when the perturbation $\delta q(t) = \delta q_0 \sin(0.5t)$ in the flow rate is applied, keeping the input pressure constant in time. The parameters are the same as in the perturbation in pressure except the friction factor, which has been chosen $\lambda = 0.01$ for this experiment,

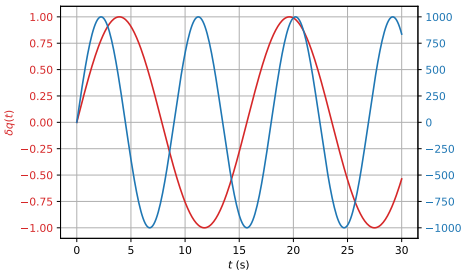

(a) Perturbations in pressure and flow

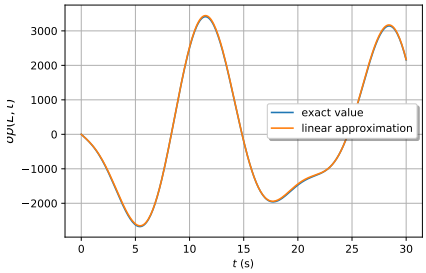

(b) Comparison between the exact output pressure and the linear approximation

Figure 6.3: Perturbation in pressure and flow and comparison between the exact output pressure and the linear approximation

yielding an approximate output pressure of $p_{20} = 4950891$ Pa. The results are similar to Figure 6.1, the relative error increasing for larger amplitudes of the flow. For relatively small values of flow rate the relative error becomes negligible.

Once perturbations in pressure and flow rate have been analyzed individually, it is worth considering the effect of perturbations in both pressure and flow rate given by expression (6.19). Figure 6.3a contains the perturbations in flow rate and pressure over time, and Figure 6.3b contains the time evolution of the pressure at the end of the pipe given by the exact value and by the linear approximation. The rest of the parameters are the same as in the perturbation in flow of the last subsection. It is evident that the linear approximation provides with very accurate results for the amplitudes chosen, being the values for the pressure at the end indistinguishable from the exact solution. It is also noticeable that, even though the behavior of the pressure is fairly complicated due to simultaneous variations in input pressure and flow rate, the linear model successfully captures the behavior of the system.

From the previous analysis it can be concluded that the linear approximation of the response of the algebraic model has a good agreement with the exact behavior for small perturbations. Therefore, the linear approximation for the algebraic model can be safely used, significantly simplifying the analytical analysis of transient behavior in gas networks.

6.3. NON-DISSIPATIVE TRANSIENT BEHAVIOR ON HYBRID NETWORKS

The coupling between transient models and the algebraic model has been discussed in Chapter 5. The results of this chapter only focused on the steady-state solution. However, it is expected that networks with pipes modeled with a mixture of transient and algebraic models exhibit a different dynamical behavior from a a network exclusively modeled with the isothermal Euler equations.

One of the goals of this chapter is to find analytical solutions to the time-dependent transport problem and compare them with the numerical results. A perturbation in pressure given by a Gaussian pulse will be applied at the input node of the networks

considered. This perturbation can be written as:

$$\psi(x,t,c,s) = \hat{p}e^{-\frac{(x-ct+s)^2}{2\sigma^2}} = \psi(x-ct+s) \tag{6.20}$$

It can be checked that this perturbation is a solution to the wave equation for pressure. The value of σ has been chosen 500. It is interesting to derive certain analytical properties of this solution which will simplify both the notation and the theoretical analysis. Consider the three pipes network. For computing the transmitted wave in the second pipe it is enough to consider a time shift of $\frac{L}{c}$, which is the time taken by the perturbation to propagate through the first pipe. Applying this time shift yields:

$$\psi\left(x,t-\frac{L}{c},c,0\right) = \psi\left(x-c\left(t-\frac{L}{c}\right)\right) = \psi(x-ct+L) = \psi(x,t,c,L) \tag{6.21}$$

and therefore the expression for the transmitted wave in the second pipe is given by $\psi(x,t,c,L)$. The reflected wave in the third pipe after the perturbation reaches the end of the network can be derived in a similar manner. However, the speed of sound will have negative sign and the perturbation will start in the rightmost side of the pipe. This is equivalent to apply a spatial shift given by L as well as a time shift given by $\frac{3L}{c}$. This can be expressed as:

$$\psi\left(x-L,-c,t-\frac{3L}{c},0\right) = \psi\left(x-L+c\left(t-\frac{3L}{c}\right)\right) = \psi(x,t,-c,-4L) \tag{6.22}$$

and therefore the reflected wave in pipe 3 is given by $\psi(x,t,-c,-4L)$.
A simplification of the notation can be introduced by removing the dependence of the function ψ with x and t. This function will of course depend on these variables, but they will be omitted for simplicity. The notation introduced is then:

$$\psi(c,s) \equiv \psi(x,t,c,s) \tag{6.23}$$

$$\psi_L(c,s) \equiv \psi(L,t,c,s) \tag{6.24}$$

The second expression will be useful when considering the algebraic model. The more general case of n pipes connected in series can be treated in an analogous way. For computing the incident wave at pipe n it is convenient to consider the time taken by the perturbation to reach pipe n, $t_0 = \frac{(n-1)L}{c}$. Applying this time shift yields:

$$\psi\left(x,t-\frac{(n-1)L}{c},c,0\right) = \psi(c,(n-1)L) \tag{6.25}$$

In a similar manner, the reflected wave at pipe n can be calculated by applying a time shift of $t_0 = \frac{nL}{c}$, which is the time that takes the perturbation to reach the end of the network. Since the reflected wave starts in the rightmost end of pipe n, a spatial shift of L also needs to be applied. The resulting expression is given by:

$$\psi\left(x-L,t-\frac{nL}{c},-c,0\right) = \psi(-c,-(n+1)L) \tag{6.26}$$

If the second pipe is modeled with the algebraic pipe, the pressure will remain constant along the pipe and equal to the pressure at the rightmost end of pipe 1. With the notation introduced above the pressure at pipe 2 can be written as $\psi_L(c,0)$.

In the reminder of this chapter a comparison between the behavior obtained by the analytical analysis and the results of numerical simulations will be done for different benchmark networks.

6.3.1. THREE PIPES

The first configuration of interest is the case of three pipes in series as seen in Figure 5.5. A simple case is when the three pipes are modeled with the semilinear model. From the analysis of the transmission and reflection coefficients in section 6.1.1 it is expected that the incoming wave is transmitted from pipe to pipe, reflection waves not being present in this configuration except at the third pipe. The analytical solution in this case will be given by:

$$\delta p(x,t) = \begin{cases} \psi(c,0) & x \in [a_1, b_1] \\ \psi(c,L) & x \in [a_2, b_2] \\ \psi(c,2L) + \psi(-c,-4L) & x \in [a_3, b_3] \end{cases}$$

Figure 6.4 contains the time evolution of a perturbation in pressure applied at the input node of pipe 1. The x axis indicates the time coordinate, and the y axis the spatial profile of the system. The parameters used in the simulation are the same as in table 3.1 except $\tau = 0.1$ seconds. All the pipes have the same length $L = 2500$ meters and the amplitude of the perturbation applied is $\tilde{p} = 1000$ Pa.

The slope of the isolines observed is equal to the speed of sound and, since all the pipes share the same geometrical and physical parameters, it is the same for all the pipes.

Since the flow rate is fixed at the output node reflection is only expected at the output node of the system, being the flow rate reflected with change of sign and the pressure increasing at the output node until twice the amplitude of the perturbation, this being observed in both the numerical and analytical solutions. The analytical solution is in good agreement with the results of the numerical simulations.

A more interesting configuration is when pipe 2 is modeled using the algebraic model. As mentioned before, since the relation between the pressure and flow rate is purely algebraic, any perturbation in one or more of these variables will propagate instantaneously to the pipes connected to the algebraic pipe.

The incoming perturbation travels at the speed of sound through pipe 1 until reaching pipe 2. Due to the conservation of mass-flow rate and the continuity of pressure at the node the evolution of the pressure and flow rate in pipe 2 is equal to the pressure and flow rate at the end of pipe 1. Moreover, this perturbation is instantaneously propagated to the end of pipe 2, immediately affecting the pressure and flow rate in pipe 3. From this theoretical analysis the analytical solution for this configuration can be derived as:

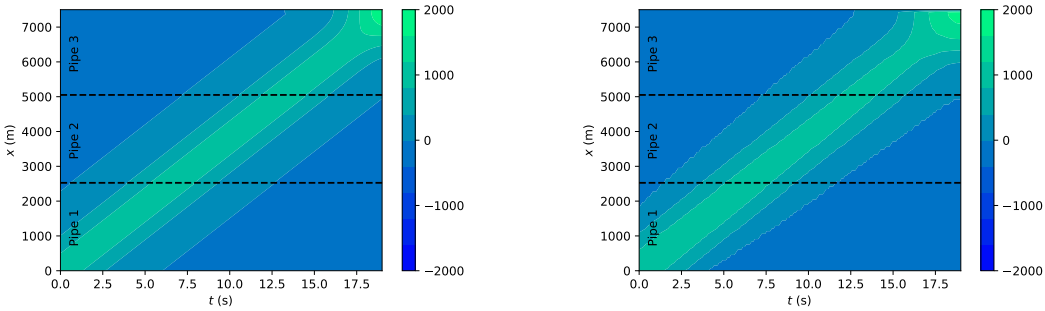

(a) Analytical solution

(b) Numerical solution

Figure 6.4: Comparison between the analytical and numerical evolution of a perturbation in pressure for configuration $1,2,3 \in \mathscr{J}_{semi}$ of the three pipes network

$$\delta p(x,t) = \begin{cases} \psi(c,0) & x \in [a_1, b_1] \\ \psi_L(c,0) & x \in [a_2, b_2] \\ \psi(c,L) + \psi(-c,-3L) & x \in [a_3, b_3] \end{cases}$$

Figure 6.5 contains the analytical and numerical solution when the second pipe is modeled with the algebraic model. It is noticeable that the perturbation reaches the end of the system in $\frac{2}{3}$ the time that it takes to reach this point when the system is modeled with the semilinear model, as expected. It is also remarkable that no reflection is observed when the perturbation enters pipe 2. The algebraic model merely acts as a modified coupling condition between pipe 1 and 3.

From this experiment it can be concluded that including the algebraic model can significantly affect the behavior of the system in this simple setting. It also becomes interesting to study the effects of including the algebraic model in more complicated gas networks.

6.3.2. Y-SHAPED

Another configuration of interest is given in Figure 5.1, where an input pipe is connected with two output pipes. This configuration is simple to study yet it offers important features for studying phenomenology present in more complex networks. It can also offer insight on the effects of introducing pipes described by the algebraic model.

For the first experiment the three pipes will be modeled with the semilinear model. It becomes necessary to analyze the behavior of the perturbation once it reaches the junction. In particular, reflection and transmission coefficients can be derived. As discussed in Chapter 5, two coupling conditions are applied at an inner node, namely the conservation of mass and the continuity of pressure. In the case of the Y-shaped net-

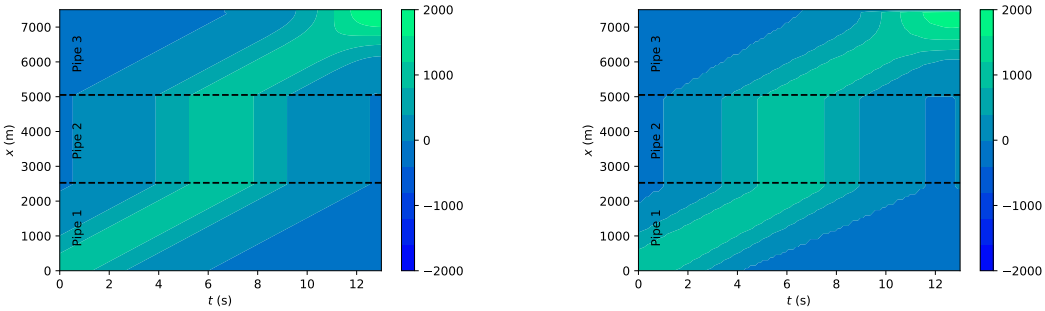

(a) Analytical solution

(b) Numerical solution

Figure 6.5: Comparison between the analytical and numerical evolution of a perturbation in pressure for configuration $1,3 \in \mathcal{J}_{semi}$ and $2 \in \mathcal{J}_{alg}$ of the three pipes network

work, these conditions can be written as:

$$q_1(0,t) = q_2(0,t) + q_3(0,t) \tag{6.27a}$$
$$p_1(0,t) = p_2(0,t) \tag{6.27b}$$
$$p_1(0,t) = p_3(0,t) \tag{6.27c}$$

where it is assumed that $x = 0$ at the junction for simplicity. Even though the mass-flow rate and pressure are coupled variables in the semilinear model, it would be convenient to reduce the analysis to only one of them. This will be possible by considering the continuity equation (6.1a). By rearranging the terms of this expression the time derivative of the pressure can be written in terms of the spatial derivative of the flow rate as:

$$\frac{\partial p}{\partial t} = -\frac{c^2}{A}\frac{\partial q}{\partial x} \tag{6.28}$$

The continuity conditions for the pressure can be differentiated with respect to time and equation (6.28) can be used for writing these conditions in terms of the spatial derivative of the mass-flow rate. Assuming that the three pipes share the same diameter and propagation speeds, the coupling conditions for the pressure can be written as:

$$\left.\frac{\partial q_1}{\partial x}\right|_{x=0} = \left.\frac{\partial q_2}{\partial x}\right|_{x=0} \tag{6.29a}$$
$$\left.\frac{\partial q_1}{\partial x}\right|_{x=0} = \left.\frac{\partial q_3}{\partial x}\right|_{x=0} \tag{6.29b}$$

and therefore are equivalent to imposing continuity in the first spatial derivative of the flow rate. This allows to calculate transmission and reflection coefficients with the

same approach as in section 6.1.1 of this chapter. An incoming and reflected wave will be assumed in pipe 1, and transmitted waves are considered in pipes 2 and 3:

$$q_1(x,t) = q_I\left(t - \frac{x}{c}\right) + q_R\left(t + \frac{x}{c}\right) \tag{6.30}$$

$$q_2(x,t) = q_2\left(t - \frac{x}{c}\right) \tag{6.31}$$

$$q_3(x,t) = q_3\left(t - \frac{x}{c}\right) \tag{6.32}$$

By imposing the coupling conditions for the flow rate derived in this section it is possible to construct a system of equations which involves incident, transmitted and reflected amplitudes as:

$$q_I(t) + q_R(t) = q_2(t) + q_3(t) \tag{6.33}$$

$$-\frac{1}{c}\frac{\partial q_I}{\partial x}(t) + \frac{1}{c}\frac{\partial q_R}{\partial x}(t) = -\frac{1}{c}\frac{\partial q_2}{\partial x}(t) \tag{6.34}$$

$$\frac{\partial q_2}{\partial x}(t) = \frac{\partial q_3}{\partial x}(t) \tag{6.35}$$

By integrating the last two equations of the system it is possible to express the amplitude of the transmitted and reflected waves in terms of the amplitude of the incoming wave:

$$q_R(t) = \frac{1}{3} q_I(t) \tag{6.36}$$

$$q_2(t) = q_3(t) = \frac{2}{3} q_I(t) \tag{6.37}$$

and therefore the transmission and reflection coefficients for the flow at the junction of the Y-shaped network are $\frac{2}{3}$ and $\frac{1}{3}$ respectively. Therefore, the reflected flow rate will preserve its sign. However, given the relation between flow rate and pressure given by $q = \frac{A}{c} p$ it is expected that the reflected pressure wave has negative amplitude since the sign of the speed of sound is reversed. The analytical expression for the perturbation can be written as:

$$\delta p(x,t) = \begin{cases} \psi(c,0) - \frac{1}{3}\psi(-c,-2L) + \frac{1}{3}\psi(c,-2L) & x \in [a_1, b_1] \\ \frac{2}{3}\left[\psi(c,L) + \psi(-c,-3L)\right] & x \in [a_2, b_2], [a_3, b_3] \end{cases}$$

where the reflection at the leftmost end of pipe 1 of the reflected wave at the junction has also been taken into account.
Figure 6.6b shows the numerical solution for the time evolution of the pressure profile. The parameters of the numerical simulation are the same as for the three pipes network. The incoming perturbation travels along pipe 1 until reaching the junction, and then it is transmitted to pipes 2 and 3. Only a fraction of the incoming amplitude is transmitted to these pipes, and a reflection with negative amplitude is also observed.

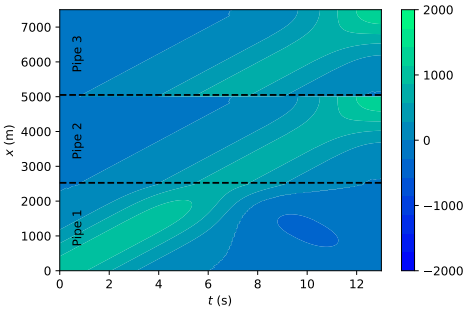

(a) Analytical solution

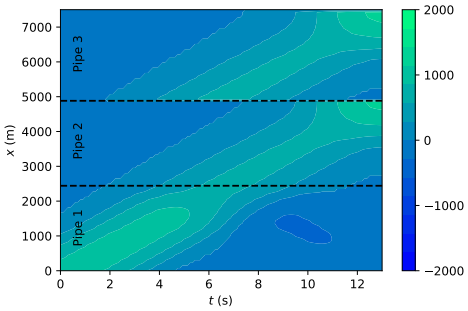

(b) Numerical solution

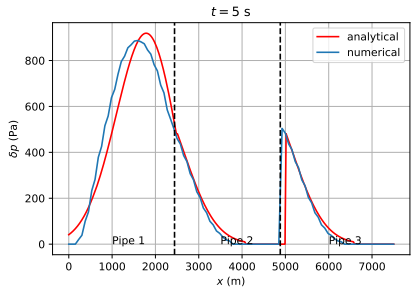

(c) Comparison between the analytical and numerical pressure profiles for $t = 5$ s

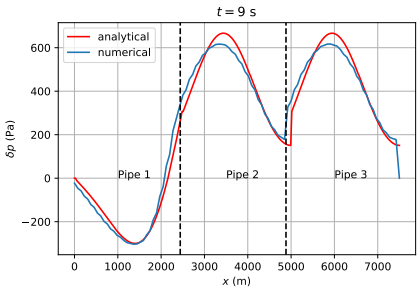

(d) Comparison between the analytical and numerical pressure profiles for $t = 9$ s

Figure 6.6: Comparison between the analytical and numerical evolution of a perturbation in pressure for configuration $1,2,3 \in \mathscr{J}_{semi}$ of the Y-shaped network

These amplitudes show a good agreement with the ones derived via the computation of the transmission and reflection coefficients, being the analytical solution depicted in Figure 6.6a.

From the previous results it can be concluded that reflection and transmission of perturbations are expected in real gas networks, the transient models being able to accurately describe this phenomenon. Moreover, it is often possible to calculate analytically the reflection and transmission coefficients.

Another case of interest is when one of the output pipes of the Y-shaped network is described by the algebraic model. Apart from the perturbations propagating instantaneously in this pipe, a different behavior regarding transmission and reflection of incoming perturbations is expected. The boundary conditions for the output pipes is the flow rate, i.e., the flow rate is fixed at the end of the output pipes. Moreover, the algebraic model assumes that the flow rate is constant along the pipe, and therefore the flow rate of an algebraic output pipe will be fixed to the boundary value. Since the flow rate of the output pipe cannot change, any perturbation in flow reaching the junction will propagate to pipe 3. Therefore, the transmitted wave has the same amplitude as the

incident wave, and no reflection of the incoming wave is expected. This behavior can be expressed analytically as:

$$\delta p(x,t) = \begin{cases} \psi(c,0) & x \in [a_1, b_1] \\ \psi_L(c,0) & x \in [a_2, b_2] \\ \psi(c,L) + \psi(-c,-3L) & x \in [a_3, b_3] \end{cases}$$

It turns out that this expression is identical to the three pipes network when pipe 2 is described by the algebraic model. The analytical time evolution of a perturbation in pressure is contained in Figure 6.7a, and the numerical results in Figure 6.7b. The plots show good agreement between the analytical and the simulation results.
From the results and discussion it is clear that using the algebraic model can affect significantly the transient behavior of a given network. Moreover, the analysis on the Y-shaped network highlights some important features of transients in gas networks. Reflected and transmitted waves are expected in junctions containing more than two pipes. However, the algebraic model effectively acts as a modification of the boundary conditions of the pipes it is connected to, not presenting any physical effects such as reflection and transmission of waves.

6.3.3. CIRCULAR

The experiments discussed in the previous sections demonstrated some interesting features of transients in gas networks. Even though the networks studied are simple, they serve to highlight the physics of the system, being able to even derive analytical solutions which show good agreement with the numerical experiments. Moreover, the role of the algebraic model as a modified boundary condition has been demonstrated as well as the effects on the transient behavior of the networks.
Once the relevant phenomenology is well understood, more complex networks can be studied. Figure 6.8 shows a gas network which will be referred as the circular network in this study due to its inner loop. This network is still simple enough that can be treated analytically, yet it offers an interesting benchmark for testing hybrid modeling approaches.
As in with the rest of network instances, the network will first be analyzed assuming that all the pipes are described with the semilinear model. The perturbation in pipe 1 will propagate until reaching the junctions and part of it will transmit to pipes 2 and 3 and part of it will be reflected. By a reasoning analogous to the Y-shaped network, the transmission coefficients for pipes 2 and 3 can be derived to be $\frac{2}{3}$, and the reflection coefficient in pipe 1 will be equal to $-\frac{1}{3}$. The reflected wave will travel backwards to the input node, where it will be reflected with a change of sign since the pressure is fixed. The transmitted waves in pipes 2 and 3 will reach the next junctions, and $\frac{2}{3}$ of the incoming amplitudes will be transmitted to pipes 4, 5 and 6. Reflection in pipes 2 and 3 will also be present. The transmitted waves from pipes 2 and 3 at pipe 4 will travel at finite speed in opposite directions and will interfere constructively at the middle point of pipe 4. The amplitudes in pipes 5 and 6 are $\frac{2}{3}$ of the amplitudes of pipes 2 and 3, and therefore are $\frac{4}{9}$ of the amplitude of the original perturbation in pipe 1. The analytical expression in this case is given by:

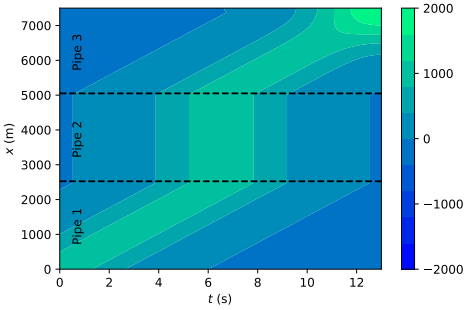

(a) Analytical solution

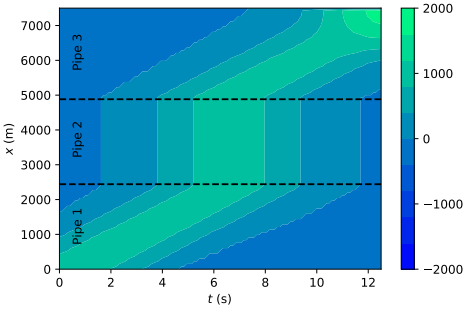

(b) Numerical solution

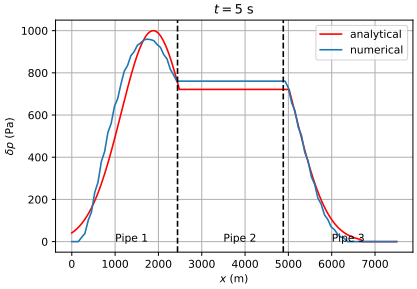

(c) Comparison between the analytical and numerical pressure profiles for $t = 5$ s

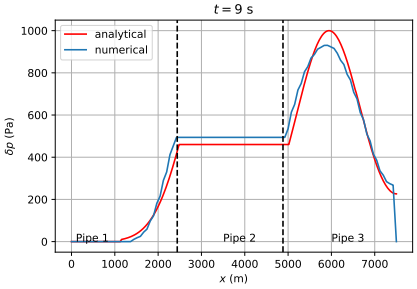

(d) Comparison between the analytical and numerical pressure profiles for $t = 9$ s

Figure 6.7: Comparison between the analytical and numerical evolution of a perturbation in pressure for configuration $1,3 \in \mathcal{J}_{semi}$ and $2 \in \mathcal{J}_{alg}$ of the Y-shaped network

$$\delta p(x,t) = \begin{cases} \psi(c,0) - \frac{1}{3}\psi(-c,-2L) + \frac{1}{3}\psi(c,-2L) & x \in [a_1,b_1] \\ \frac{2}{3}\psi(c,L) - \frac{2}{9}\psi(-c,-3L) & x \in [a_2,b_2],[a_3,b_3] \\ \frac{4}{9}\left[\psi(c,2L) + \psi(-c,-3L)\right] & x \in [a_4,b_4] \\ \frac{4}{9}\left[\psi(c,2L) + \psi(-c,-4L)\right] & x \in [a_5,b_5],[a_6,b_6] \end{cases}$$

A comparison between the analytical and numerical time evolution of the pressure profiles is contained in Figure 6.9. The parameters are the same as for the rest of the networks in this chapter. The analytical and numerical solutions show good agreement for the transient behavior of the network.

Once the transient behavior of the circular network have been studied using exclusively the semilinear model, it is of interest to study the network with a configuration combining both transient and algebraic models. The configuration chosen will be pipes 1,3,5 and 6 described by the semilinear model and pipes 2 and 4 with the algebraic model. As with the network fully described by the semilinear model, the perturbation in pipe 1 will propagate until reaching the first junction. Part of the incoming perturbation will be transmitted to pipe 3 with finite speed and part will be reflected. On the other hand, since pipe 2 is described by the algebraic model the perturbation will propagate instantaneously to the junction between the pipes 2, 4 and 6. The resulting perturbation will transmit at finite speed in pipe 6 eventually reaching the end of the network. Since pipe 4 is modeled with the algebraic model, the perturbation coming from pipe 2 will propagate instantaneously to the junction between the pipes 3, 4 and 5 as well. This perturbation will be transmitted to pipes 3 and 5, where it will travel at finite speed since these pipes are modeled with the semilinear model. Therefore, the perturbation

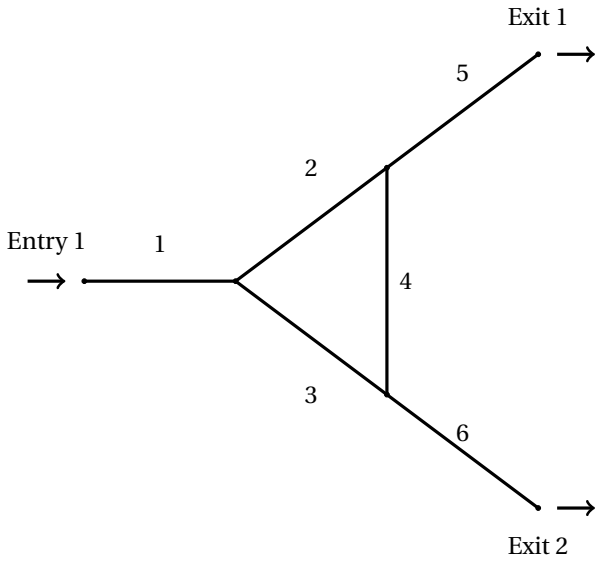

Figure 6.8: Circular network

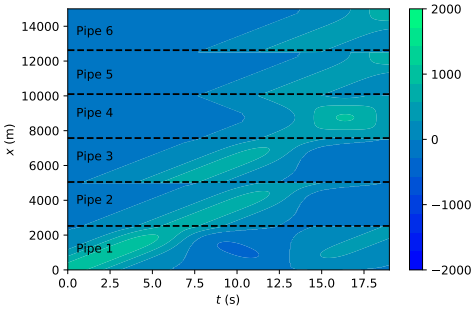

(a) Analytical solution

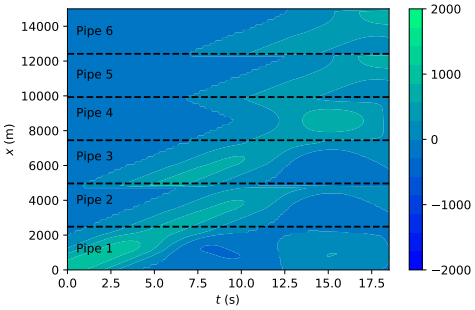

(b) Numerical solution

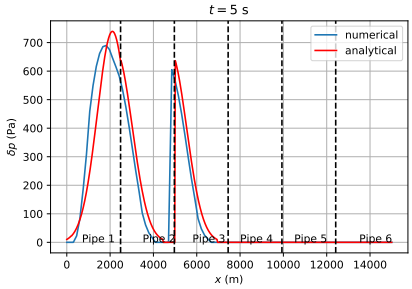

(c) Comparison between the analytical and numerical pressure profiles for $t = 5$ s

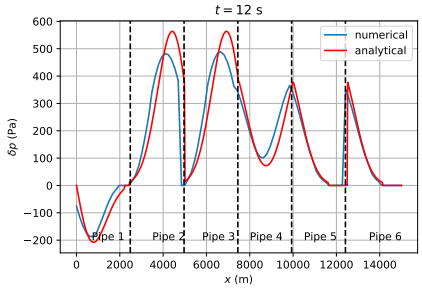

(d) Comparison between the analytical and numerical pressure profiles for $t = 12$ s

Figure 6.9: Comparison between the analytical and numerical evolution of a perturbation in pressure for configuration $1,2,3,4,5,6 \in \mathcal{J}_{semi}$ of the circular network

at the end of pipe 1 will effectively propagate to the semilinear pipes 3, 5 and 6. Moreover, it is clear that this perturbation will affect both ends of pipe 3, being two waves traveling in opposite directions. Therefore the perturbation at the end of pipe 1 will be 'split' into four pipes, pipes 5, 6 and both ends of pipe 3. This needs to be taken into account for computing the transmission and reflection coefficients in the analytical solution. Considering that pipe 1 is effectively connected to four pipes, the conservation of mass-flow rate at the junction can be written as:

$$q_1(t,0) = \sum_{i=2}^{4} q_i(t,0) \tag{6.38}$$

$$q_4(x,t) = q_4\left(t - \frac{x}{c}\right) \tag{6.39}$$

where the fourth pipe is actually the rightmost end of pipe 3. Assuming that q_1 is a sum of an incident and a reflected wave, imposing the continuity of the first derivative for the flow and integrating:

$$q_I + q_R = \sum_{i=2}^{4} q_i \tag{6.40}$$

$$q_I - q_R = q_2 \tag{6.41}$$

$$q_3 = q_4 = q_2 \tag{6.42}$$

from where the transmitted and reflected amplitudes can be expressed in terms of the incident amplitude as:

$$q_R(t) = \frac{1}{2} q_I(t) \tag{6.43}$$

$$q_2(t) = q_3(t) = q_4(t) = \frac{1}{2} q_I(t) \tag{6.44}$$

This result states that the transmission coefficients for the pressure will be equal to $\frac{1}{2}$, being the reflection coefficient equal to $-\frac{1}{2}$. Once the transmission and reflection coefficients have been derived, it is possible to write the analytical solution as:

$$\delta p(x,t) = \begin{cases} \psi(c,0) - \frac{1}{2}\psi(-c,-2L) + \frac{1}{2}\psi(c,-2L) & x \in [a_1, b_1] \\ \frac{1}{2}\psi_L(c,0) & x \in [a_2, b_2], [a_4, b_4] \\ \frac{1}{2}\left[\psi(c,L) + \psi(-c,-2L)\right] & x \in [a_3, b_3] \\ \frac{1}{2}\left[\psi(c,L) + \psi(-c,-3L)\right] & x \in [a_5, b_5], [a_6, b_6] \end{cases}$$

Figure 6.10 compares the analytical and numerical solutions when pipes 2 and 4 are described by the algebraic model.The constructive interference at pipe 3 resulting from perturbations traveling in opposite directions in this pipe can be observed clearly.

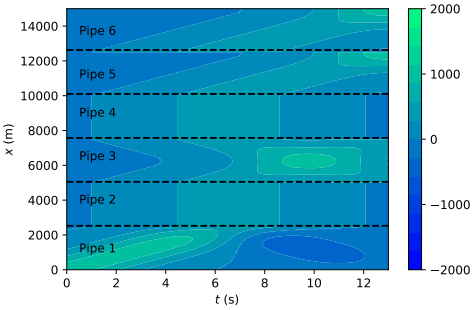

(a) Analytical solution

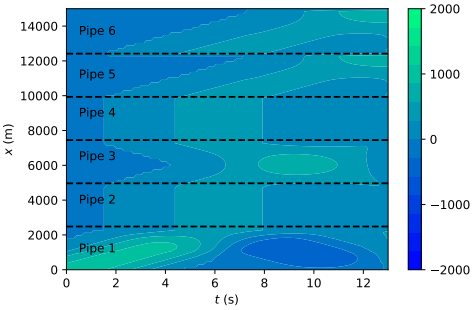

(b) Numerical solution

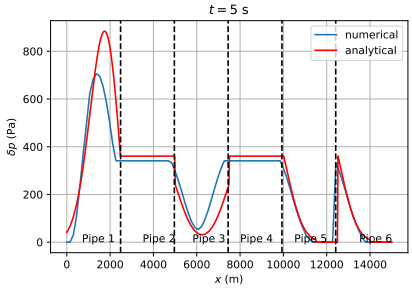

(c) Comparison between the analytical and numerical pressure profiles for $t = 5$ s

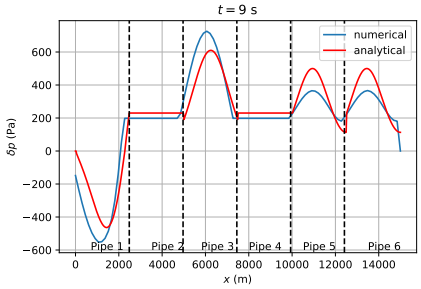

(d) Comparison between the analytical and numerical pressure profiles for $t = 9$ s

Figure 6.10: Comparison between the analytical and numerical evolution of a perturbation in pressure for configuration $1,3,5,6 \in \mathcal{J}_{semi}$ and $2,4 \in \mathcal{J}_{alg}$ of the circular network

It is evident that modeling pipe 2 and 4 with the algebraic model changes the transient behavior of the network significantly. In particular, for the circular network the constructive interference has been shifted from pipe 4 to pipe 3. This is due to the instantaneous propagation of perturbations for the algebraic model. One of the consequences of this is that perturbations take less time in reaching parts connected by algebraic pipes than if these pipes were described by a transient model.

Moreover, no physical effects such as transmission and reflection of waves are observed in the algebraic pipes. The algebraic model acts as a 'bridge' between the pipes by coupling pipes that aren't physically connected. Therefore the algebraic model can be interpreted as a modification of the coupling conditions of the pipes connected to it. This effect needs to be taken into account for computing the transmission and reflection coefficients for the pipes governed by a transient model, as it has been discussed in this section.

6.4. DISSIPATIVE TRANSIENT BEHAVIOR

In the previous section the transient behavior was analyzed without friction. This greatly simplified the problem allowing to find simple analytical solutions. The goal of this section is to find an analytical expression for describing the evolution of the pressure profile when dissipative effects are considered. The semilinear model was the model chosen in the non-friction case since it admits analytical solutions. Due to its simplicity it will also be the model of choice for this section. With the aim of simplifying the problem the friction term will be linearized by taking a perturbative approach.
Assuming that the flow rate is positive and that the pipes are horizontal so the gravity term can be dropped, the semilinear model can be written as:

$$\frac{1}{c^2}\frac{\partial p}{\partial t}+\frac{1}{A}\frac{\partial q}{\partial x}=0 \tag{6.45a}$$

$$\frac{1}{A}\frac{\partial q}{\partial t}+\frac{\partial p}{\partial x}=-\alpha\frac{q^2}{p} \tag{6.45b}$$

where $\alpha \equiv \frac{RTz}{2DA^2}\lambda$. We observe that the friction term is nonlinear, and since this system of PDEs doesn't admit an analytical solution easily a perturbative approach will be taken. The goal of this is to linearize the resulting system for the perturbation with the aim of obtaining an analytical solution.
As in previous sections, a perturbation in flow rate and pressure of the form $q = q_0 + \delta q$ and $p = p_0 + \delta p$ is taken, where q_0 and p_0 are the steady-state mass-flow rate and pressure respectively, and the perturbations δq and δp satisfy $\frac{\delta q}{q_0} \ll 1$ and $\frac{\delta p}{p_0} \ll 1$. The perturbations are small enough such that only first order terms are kept, and therefore the term in the right hand side of equation (6.45b) can be linearized as:

$$\frac{q^2}{p}\simeq\left(\frac{1}{p_0}-\frac{\delta p}{p_0^2}\right)\left(q_0^2+2q_0\delta q\right)\simeq\frac{q_0^2}{p_0}-\frac{q_0^2}{p_0^2}\delta p+\frac{2q_0}{p_0}\delta q \tag{6.46}$$

It is assumed that the steady-state pressure and flow rate don't depend on space and time, so the partial derivatives of these terms are equal to zero. The resulting system will only contain terms proportional to the perturbations. The linearized friction term also needs to be included. The term which is not proportional to the perturbation can be neglected since the rest of the terms of the system are proportional to the perturbation. After these approximations the resulting system can be written as:

$$\frac{1}{c^2}\frac{\partial\delta p}{\partial t}+\frac{1}{A}\frac{\partial\delta q}{\partial x}=0 \tag{6.47a}$$

$$\frac{1}{A}\frac{\partial\delta q}{\partial t}+\frac{\partial\delta p}{\partial x}=\alpha\frac{q_0^2}{p_0^2}\delta p-\alpha\frac{2q_0}{p_0}\delta q \tag{6.47b}$$

This system is still a partial differential equation for the perturbations in flow rate and pressure. Although it is not a homogeneous system, it is linear. In the next subsections we will describe two procedures for finding solutions to this system.

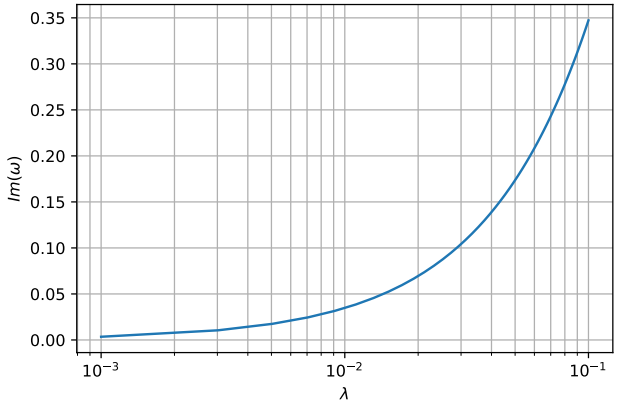

Figure 6.11: Imaginary part of ω with respect to the friction factor calculated using (6.50)

6.4.1. LINEAR SYSTEM FOR FLOW RATE AND PRESSURE

The approach presented in this section was also used in [22] for computing the attenuation coefficient for gas flow in pipes using the Fanno model. The application of this method for the semilinear model is analogous and will be discussed in this section.
Since the system (6.47) involves both the pressure and flow rate an ansatz for these two variables of the form $\delta p = \tilde{p}e^{i(\omega t - kx)}$ and $\delta q = \tilde{q}e^{i(\omega t - kx)}$ will be taken, where $\tilde{p}$ and $\tilde{q}$ are the pressure and flow rate amplitudes and $\omega, k \in \mathbb{C}$. The real part of these quantities will be the angular frequency and wave number respectively in the case of non friction, and the imaginary parts will count for the decay in time and space due to friction.
The reason for taking this ansatz is that the time and space derivatives are proportional to the perturbations, making the analytical treatment of this system possible. Substituting the ansatzs for the pressure and flow rate and rearranging the system of equations:

$$\frac{\omega}{c^2}\delta p - \frac{k}{A}\delta q = 0 \tag{6.48a}$$

$$\left(-ik - \frac{\alpha q_0^2}{p_0^2}\right)\delta p + \left(\frac{i\omega}{A} + \frac{2\alpha q_0}{p_0}\right)\delta q = 0 \tag{6.48b}$$

This problem is an homogeneous system of equations. In order to have a non trivial solution the determinant of the matrix of coefficients need to be equal to zero, and therefore the following condition is imposed:

$$\begin{vmatrix} \frac{\omega}{c^2} & -\frac{k}{A} \\ -ik - \frac{\alpha q_0^2}{p_0^2} & \frac{i\omega}{A} + \frac{2\alpha q_0}{p_0} \end{vmatrix} = 0 \tag{6.49}$$

which is equivalent to the following second order equation for ω:

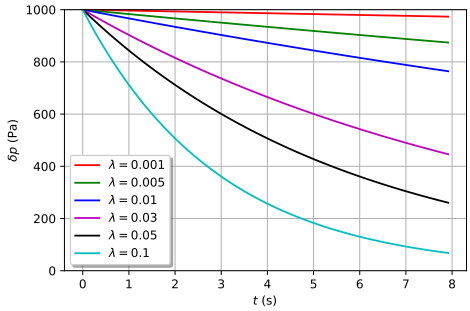

(a) Decay obtained by the theoretical analysis

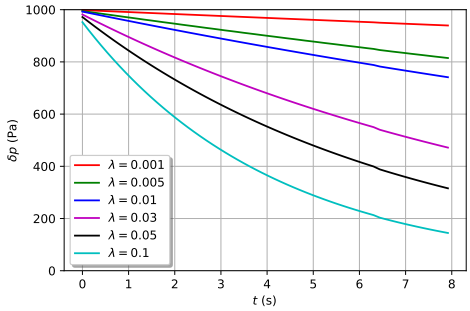

(b) Decay obtained by the numerical experiments

Figure 6.12: Decay of a perturbation in time due to friction effects

$$\frac{i}{c^2 A}\omega^2 + \frac{2\alpha q_0}{c^2 p_0}\omega - \frac{k}{A}\left(ik + \frac{\alpha q_0^2}{p_0^2}\right) = 0 \tag{6.50}$$

The resulting equation establishes a relation between ω and k. Given this relation, it is possible to obtain either the angular frequency or the wave number. The quantity of interest in this case is the imaginary part of the angular frequency, which is responsible for the decay of the wave in time due to friction. In this case the speed of sound is defined as $c = \frac{\mathrm{Re}(\omega)}{k}$.

Figure 6.11 contains the value of the decay coefficient with respect the friction factor for parameters in 3.1. The friction factor is varied in a logarithmic scale from 0.001 to 0.1, and since the relation between the decay coefficient and the logarithmic friction factor is exponential, the dependency of the decay coefficient with the friction factor is linear. The decay coefficient doesn't depend on neither the real part of ω or k, and therefore the decay is the same for all angular frequencies.

It is of interest to compare the results from the theoretical analysis with the results of the numerical simulations. This will be done by analyzing the numerical simulation of the decay of the amplitude of a perturbation in pressure for a single pipe. The parameters used for the numerical simulations are the same as in the rest of chapter. The analytical solution will consist on a traveling pulse multiplied by an exponential decay $e^{-\mathrm{Im}(\omega)t}$.

Figure 6.12 shows the maximum amplitude observed at a given time for several values of the friction factor, and therefore representing the decay of the amplitude of the perturbation. It is observed that the numerical and analytical results agree. The numerical solution seems to exhibit an slightly larger decay than the analytical for small values of friction, and this difference can be attributed to numerical errors. For small values of friction, the coefficient responsible of the decay of the perturbation is very small, and therefore producing a roughly linear decay. For higher values of the friction, the behavior is clearly exponential decay for both analytical and numerical results. It can

be concluded that the analytical solution for gas transport with friction is a good approximation that is able to describe the transient behavior observed in the numerical simulations.
The goal of the perturbation analysis carried out in this section was to compute an analytical approximation to the wave propagation problem when taking friction into account. In particular, the imaginary part of ω is of special interest since it accounts for the temporal decay due to friction.

7

Conclusion

This study was concerned with the mathematical modeling of gas transport in pipeline networks, and in particular with a hybrid modeling containing both transient and algebraic models for the pipes. Both steady-state and transient behavior were considered. In the case of transient phenomena analytical solutions to the transport problem were obtained which show good agreement with the numerical experiments.
An introduction to the physics behind gas transport is given in Chapter 2, together with a discussion and comparison of several friction factors. The comparison in Chapter 3 between the temperature-dependent Euler equations and the isothermal Euler equations in a single pipe proves that isothermal gas flow approximates well the transport of gas in pipes for the parameters considered. A family of isothermal models was proposed, namely the isothermal Euler equations, the semilinear and the algebraic model. These models were compared for a single pipe and they show to be roughly equivalent in steady state. The differences observed between the models were explained regarding the approximations made for deriving these models. In particular, it became evident that the semilinear model is equivalent to the isothermal Euler equations for high pressure and it has the advantage of being tractable analytically.
A review of existing methods for solving hyperbolic problems was presented in Chapter 4. The method chosen for this study is an implicit box scheme suitable for subsonic flow. This method is able to handle source terms, and this was particularly useful for the study of dissipative gas transport. The method is relatively simple to implement and doesn't need to fulfill the CFL condition, allowing to rapidly obtain the steady-state solution since it allows arbitrarily large time steps.
The main focus of this study was the hybrid modeling of gas pipeline networks, where different pipes are described by different models. Chapter 5 contains a discussion of the coupling conditions for isothermal models as well as numerical experiments for hybrid models in steady-state regime. The most interesting case is a network partially modeled with an algebraic model, being the rest of the network described by a transient model. In practice it is seen that there are no substantial differences between using the semilinear and algebraic model for steady state since they are equivalent in this

regime. Despite this, it was expected that using the algebraic model would have significant effects in the transient behavior of the network.

The transient behavior studied in Chapter 6 focuses on the behavior of a perturbation propagating in benchmark networks. Of particular interest were physical effects such as reflection and transmission of wave in junctions between the pipes for both full transient and hybrid models. Moreover, the effects of including pipes described by the algebraic model were extensively studied.

Since the algebraic model is a steady-state equation any change in the variables of the pipe will immediately propagate to the pipes connected to it on the other hand. Of special interest is the response of the algebraic model to an incoming perturbation in both pressure and flow rate. A first order approximation was derived by performing the Taylor expansion of the algebraic model. It was demonstrated that the first order approximation matches the exact response to the perturbations.

From the experiments performed it was concluded that pipes modeled with the algebraic model don't present physical effects such as transmission and reflection. Rather than acting as physical pipes, they act as a modified coupling condition for the transient pipes connected to them.

The calculation of transmission and reflection coefficients is straightforward in networks described with transient models by imposing the coupling conditions discussed in Chapter 5. However, special attention needs to be payed when the junction considered contains pipes described by the algebraic model. Since the algebraic pipes act as a bond between two transient pipes, for computing the transmission and reflection coefficients all the pipes modeled with a transient model affected by the perturbation need to be considered. This highlights the significant differences introduced by including the algebraic model.

Two different regimes were considered, namely non dissipative and dissipative transport, being these non-including and including friction respectively. Transport with absence of friction terms was studied analytically with the semilinear model, and in combination with the perturbation analysis of the algebraic model, an analytical solution was found for the networks considered, showing a good agreement with the results of the numerical experiments.

One of the main effects of including friction is the decay of the amplitude of perturbations in space and time. Since the analytical treatment of the transient models is unfeasible, a perturbation analysis and subsequent linearization of the friction term was performed. The dependence of the decay coefficient was analyzed for several values of the friction factor, as well as a comparison between the decay of the amplitude of the perturbation resulting from the numerical experiments and the theoretical analysis. The analytical results agree with the observations from the experiments, and we conclude that the analytical method offers a simplified description of transient phenomena in presence of friction.

Finally, based on the results of this study, we would like to indicate a few future research directions. The hierarchical modeling of realistic gas networks is a topic of interest. In [13] a hybrid simulation of a Canadian gas network was performed with the isothermal Euler equations, the semilinear model and the algebraic model, demonstrating that the behavior of the network is greatly affected by the modeling choices. It would be

desirable to explore the coupling and effects of algebraic models with other elements such as compressors and valves in complex networks. The algebraic model could be used to model short pipes in large networks since the transient behavior in short pipes can be considered instantaneous in comparison with transient behavior in long pipes due to the finite speed of sound.
In this study the coupling of algebraic models has been only considered in the subsonic case. To the best of our knowledge the study of networks with transient and algebraic models has not been studied in the supersonic regime, and we consider this a direction worth exploring. Moreover, apart from the modeling effects in the physics of the system, effects of including the algebraic model in convergence and stability of numerical schemes is still lacking.
Last, the coupling of transient and algebraic models is of interest for other domains where the system can be described as a network, such as traffic networks, blood vessel modeling and air traffic management [23]. We are positive that the results and techniques derived for gas networks modeling can be extended and generalized for these systems.

BIBLIOGRAPHY

[1] Vaclav Smil. *Natural gas: fuel for the 21st century*. John Wiley & Sons, 2015.

[2] Yunus A Cengel and Michael A Boles. "Thermodynamics: an engineering approach". In: *Sea* 1000 (2002), p. 8862.

[3] Thorsten Koch, Benjamin Hiller, and Marc E Pfetsch. *Evaluating gas network capacities*. SIAM, 2015.

[4] Maciej Chaczykowski. "Sensitivity of pipeline gas flow model to the selection of the equation of state". In: *Chemical engineering research and design* 87.12 (2009), pp. 1596–1603.

[5] E Shashi Menon. *Gas pipeline hydraulics*. Crc Press, 2005.

[6] Ning Hsing Chen. "An explicit equation for friction factor in pipe". In: *Industrial & Engineering Chemistry Fundamentals* 18.3 (1979), pp. 296–297.

[7] Mapundi K Banda, Michael Herty, and Axel Klar. "Gas flow in pipeline networks". In: *NHM* 1.1 (2006), pp. 41–56.

[8] John David Anderson and J Wendt. *Computational fluid dynamics*. Vol. 206. Springer, 1995.

[9] Maciej Chaczykowski. "Transient flow in natural gas pipeline–The effect of pipeline thermal model". In: *Applied Mathematical Modelling* 34.4 (2010), pp. 1051–1067.

[10] Andrzej J Osiadacz and Maciej Chaczykowski. "Comparison of isothermal and non-isothermal pipeline gas flow models". In: *Chemical Engineering Journal* 81.1-3 (2001), pp. 41–51.

[11] Jens Brouwer, Ingenuin Gasser, and Michael Herty. "Gas pipeline models revisited: model hierarchies, nonisothermal models, and simulations of networks". In: *Multiscale Modeling & Simulation* 9.2 (2011), pp. 601–623.

[12] Pia Domschke, Oliver Kolb, and Jens Lang. "An adaptive model switching and discretization algorithm for gas flow on networks". In: *Procedia Computer Science* 1.1 (2010), pp. 1331–1340.

[13] Mapundi K Banda and Michael Herty. "Multiscale modeling for gas flow in pipe networks". In: *Mathematical Methods in the Applied Sciences* 31.8 (2008), pp. 915–936.

[14] Liang-biao Ouyang and Khalid Aziz. "Steady-state gas flow in pipes". In: *Journal of Petroleum Science and Engineering* 14.3-4 (1996), pp. 137–158.

[15] Randall J LeVeque. *Finite volume methods for hyperbolic problems*. Vol. 31. Cambridge university press, 2002.

[16] Oliver Kolb, Jens Lang, and Pia Bales. “An implicit box scheme for subsonic compressible flow with dissipative source term”. In: *Numerical Algorithms* 53.2-3 (2010), pp. 293–307.

[17] William H Press, Saul A Teukolsky, and William T Vetterling. “Numerical recipes in C++”. In: *The art of scientific computing* 2 (1992), p. 1002.

[18] Endre Süli and David F Mayers. *An introduction to numerical analysis*. Cambridge university press, 2003.

[19] Peter Benner, Sara Grundel, and Christian Himpe. “Gas network benchmark models”. In: (2018).

[20] Mapundi K Banda, Michael Herty, and Axel Klar. “Coupling conditions for gas networks governed by the isothermal Euler equations”. In: *NHM* 1.2 (2006), pp. 295–314.

[21] Anthony Philip French. *Vibrations and waves*. CRC press, 1971.

[22] Yingfeng Meng, Hongtao Li, and Gao Li. “Investigation on propagation characteristics of the pressure wave in gas flow through pipes and its application in gas drilling”. In: *Journal of Natural Gas Science and Engineering* 22 (2015), pp. 163–171.

[23] Alberto Bressan, Sunčica Čanić, and Mauro Garavello. “Flows on networks: recent results and perspectives”. In: *EMS Surveys in Mathematical Sciences* 1.1 (2014), pp. 47–111.